Journal of Medicinal Chemistry

Article

Design, Synthesis and Preclinical Evaluation of Fused Pyrimidine-Based Hydroxamates for the Treatment of Hepatocellular Carcinoma

Dizhong Chen, Chang Kai Soh, Wei Huang Goh, and Haishan Wang

J. Med. Chem., **Just Accepted Manuscript** • DOI: 10.1021/acs.jmedchem.7b01465 • Publication Date (Web): 23 Jan 2018

ACS Publications

Journal of Medicinal Chemistry is published by the American Chemical Society. 1155 Sixteenth Street N.W., Washington, DC 20036

Design, Synthesis and Preclinical Evaluation of Fused Pyrimidine-Based Hydroxamates for the Treatment of Hepatocellular Carcinoma

Dizhong Chen,[†] *Chang Kai Soh,*[†] *Wei Huang Goh,*[†] *and Haishan Wang**[*,†,‡]

[†]Drug Development Unit, Institute of Molecular and Cell Biology, Agency for Science, Technology and Research, 61 Biopolis Drive, Proteos, Singapore 138673, Republic of Singapore

[‡]Probit Pharmaceuticals Pte. Ltd., 10 Anson Road #26-04, Singapore 079903, Republic of Singapore

ABSTRACT

Class I histone deacetylases (HDACs) are highly expressed and/or upregulated in hepatocellular carcinoma (HCC) and are associated with aggressiveness, spread, and increased mortality of HCC. Activation of phosphatidylinositol 3-kinase-Akt-mammalian target of rapamycin (PI3K/Akt/mTOR) signaling pathway was involved in the development of HCC and acquired resistance to sorafenib. A series of purine or 5H-pyrrolo[3,2-d]pyrimidine based hydroxamates were designed and developed as multi-target drugs to modulate both HDACs and the PI3K/Akt/mTOR pathway. Among 39 cell lines screened, the molecules (e.g., **20e**, **20f**, and **20q**) were the most selective against leukemia, lymphoma, and HCC cells; they also demonstrated target modulation in cancer cell lines and in mice bearing MV4-11 and HepG2 tumors. Compound **20f** in particular showed significant single agent oral efficacy in hypervascular liver

cancer models (e.g., HepG2, HuH-7, and Hep3B) and was well-tolerated. These encouraging results, along with its favorable target profile and tissue distribution, warrant further development of **20f**.

KEYWORDS. HDAC inhibitor, PI3K inhibitor, PI3K/Akt/mTOR pathway, multi-target, purine, fused-pyrimidine, hydroxamic acid, anticancer, xenograft, efficacy, hepatocellular carcinoma, liver cancer, leukemia, non-Hodgkin lymphomas.

Introduction

Hepatocellular carcinoma (HCC) is the third most fatal cancer worldwide with sorafenib being the first and only approved systemic therapy for advanced HCC since 2007.[1, 2] Only recently in April 2017 was regorafenib, a fluorinated version of sorafenib, approved to treat HCC patients who fail sorafenib treatment (sorafenib resistance).[3, 4] However there is currently no established systemic therapy for HCC patients who tolerate neither sorafenib nor regorafenib, or fail regorafenib therapy.[5] Class I histone deacetylases (HDACs) are highly expressed and/or upregulated in hepatocellular carcinoma (HCC) and are associated with aggressiveness, spread, and increased mortality of HCC.[6-9] Drug resistance to sorafenib involves pathways such as PI3K/Akt and JAK/STAT, and PI3K/Akt/mTOR signaling pathway activation has been found in a subset of HCC tumor samples.[10-13] The above data thus suggest that both HDACs and PI3K/Akt/mTOR are relevant targets for the treatment of advanced HCC.

HDACs are validated oncology targets and there are already approved HDAC inhibitors for the treatment of lymphoma and multiple myeloma (Figure 1), with new indications, including HCC, being explored and further validated in clinics.[14] In preclinical studies, both HDAC

inhibitors vorinostat (Figure 1) and *N*-hydroxy-4-[[(2S)-3-methyl-2-phenylbutanoyl]amino]benzamide (OSU-HDAC42) [15] were efficacious in HCC models, while HDAC inhibitor panobinostat (Figure 1) used in combination with sorafenib demonstrated the highest preclinical efficacy in HCC models.[16] In completed clinical trials, HDAC inhibitor belinostat (Figure 1) demonstrated disease stabilization with a tolerable toxicity profile amongst patients with HCC,[17] while resminostat (Figure 1) [14] in combination with sorafenib was found to be safe and showed early signs of efficacy in advanced HCC patients.

Both PI3K and mTOR are also validated cancer targets: currently there are two approved PI3K inhibitors: idelalisib (PI3Kδ selective)[18] and copanlisib (pan-class I PI3K inhibitor with preferential activity against PI3Kα and PI3Kδ) [19] (Figure 1). Combination of mTOR inhibitor (5-(2,4-bis((*S*)-3-methylmorpholino)pyrido[2,3-d]pyrimidin-7-yl)-2-methoxyphenyl)methanol (AZD8055) [20] with HDAC inhibitor vorinostat in vivo almost completely inhibited tumor-growth without obvious adverse effects. Furthermore, the combination of dual PI3K/mTOR inhibitor 1-[4-[4-(dimethylamino)piperidine-1-carbonyl]phenyl]-3-[4-(4,6-dimorpholin-4-yl-1,3,5-triazin-2-yl)phenyl]urea (PKI-587) [21] with sorafenib targeting both PI3K/AKT/mTOR and Ras/Raf/MAPK pathways showed synergistic inhibition of HCC cell proliferation. These results suggest that it is feasible and effective to target both HDACs and PI3K/AKT/mTOR pathways together for the treatment to advanced HCC.

From a medicinal chemist's perspective, a multi-target drug (single molecule) is an alternative approach to achieve multi-targeted therapy as compared to combination therapy (multiple molecules). Based on our knowledge and experience in the development of HDAC inhibitors [22-24] and PI3K/mTOR inhibitors (e.g., SB2343 (**1**), Figure 1),[25, 26] we designed and synthesized a

series of fused-pyrimidine based hydroxamates to target both HDACs and the PI3K/Akt/mTOR pathway for the treatment of cancer as well as non-oncology applications.[27]

As illustrated in Figure 1, a typical HDAC inhibitor (vorinostat) comprises of three parts: zinc-binding group (ZBG), linker, and a lipophilic and surface recognition "CAP" group. As the CAP sits outside of the binding pocket of HDAC enzymes,[28] it can be replaced with a kinase inhibitor core structure to afford a novel HDAC-kinase inhibitor.[29] Purine and fused-pyrimidine are scaffolds used to build up competitive kinase inhibitors (e.g., **1** (SB2343), PI103 (**2**),[30] pictilisib,[30-32] Figure 1) which compete with adenosine triphosphate (ATP). Hence, the HDAC inhibitor moieties (linker + ZBG) can be used to replace the sugar part of ATP to construct a kinase-HDAC inhibitor. The general chemical types of the designed HDAC-PI3K/mTOR inhibitors are depicted in Figure 2. Previous SAR studies on purine-based PI3K/mTOR inhibitors (**4**, as analogues of **1**, Figure 2) had shown that the 9-position can accommodate rings and chains,[26] thus HDAC inhibitor moieties were introduced to the 9-position to generate HDAC-PI3K/mTOR inhibitors (**5**). Because both Cpd-38 (**6**) and Cpd-51 (**8**) (Figure 2), [26] two representative examples of **4**, are potent PI3K and mTOR inhibitors, two expanded chemical series **7** and **9** were designed to establish the SARs for HDAC, PI3K and mTOR inhibitory activities as well as tune target profile (HDAC vs PI3K vs mTOR) by exploring a variety of combination of functional groups (i.e., Linker, and R^2) (Figure 2). Series **10** was designed to explore potential morpholine replacement. As the best combination profile of HDAC/PI3K/mTOR is unknown or yet to be validated, the inhibitors were designed to have a broad range of potency or strength against each target (i.e., HDAC, PI3K, and mTOR) in order to mimic the combination of single-target inhibitors. The optimal combination was then determined in preclinical studies. Even though every drug candidate has to address its toxicity pre-clinically,

there remain concerns of potential combined toxicity of designed multi-target drugs in clinics. Fortunately, the latest Phase I results of CUDC-907 (**3**) (Figure 1) demonstrated tolerability and antitumor activity across all dosing schedules studied in patients with relapsed or refractory lymphoma or multiple myeloma.[33, 34] **3** (CUDC-907) [35] is the first HDAC/PI3K dual inhibitor entered clinical trials,[34, 36, 37] being considered as a hybrid derivative of PI3K inhibitor pictilisib and HDAC inhibitor quisinostat (Figure 1). [38, 39]

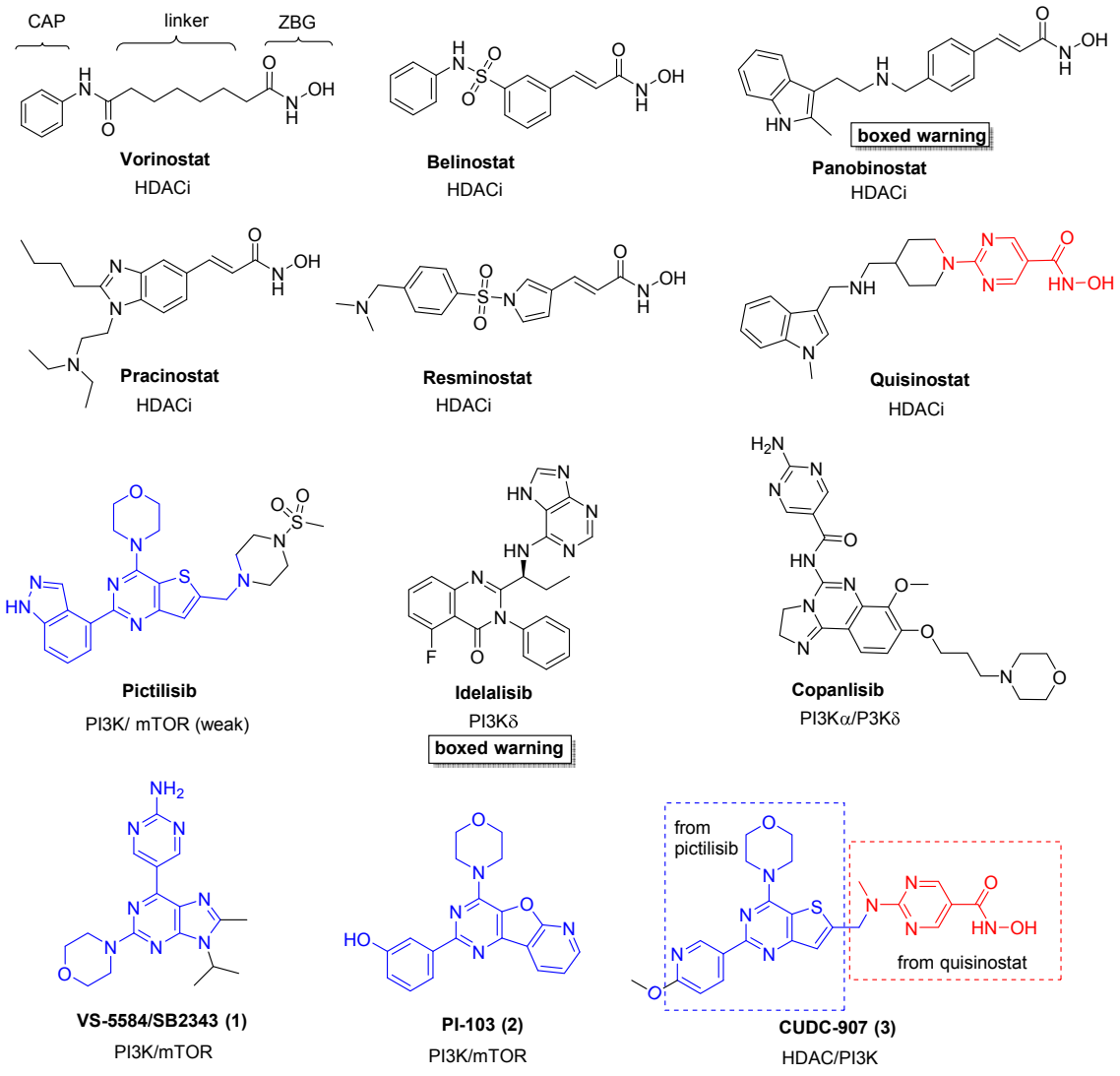

Figure 1. Examples and chemical structure features of HDAC inhibitors (HDACi), PI3K/mTOR inhibitors, and HDAC/PI3K dual inhibitor. **3** (CUDC-907) is considered to be a hybrid derivative

of pictilisib and quisinostat. Both idelalisib and panobinostat were issued with a boxed warning by FDA.

Here we report the synthesis and preclinical evaluation of hydroxamates **7**, **9** and **10** series (Figure 2) which have been designed and developed to modulate both HDACs and the PI3K/Akt/mTOR pathway. Among 39 cancer cell lines screened, the molecules (e.g., **20e**, **20f**, and **20q**) were more potent against leukemia, lymphoma, and HCC cells; they also demonstrated target modulation in cancer cell lines and in mice bearing MV4-11 and HepG2 tumors. Compound **20f** in particular showed significant single agent oral efficacy in hypervascular HCC models (e.g., HepG2, HuH-7, and Hep3B) and was well-tolerated. These encouraging results, along with its favorable target profile and tissue distribution, warrant further development of **20f**.

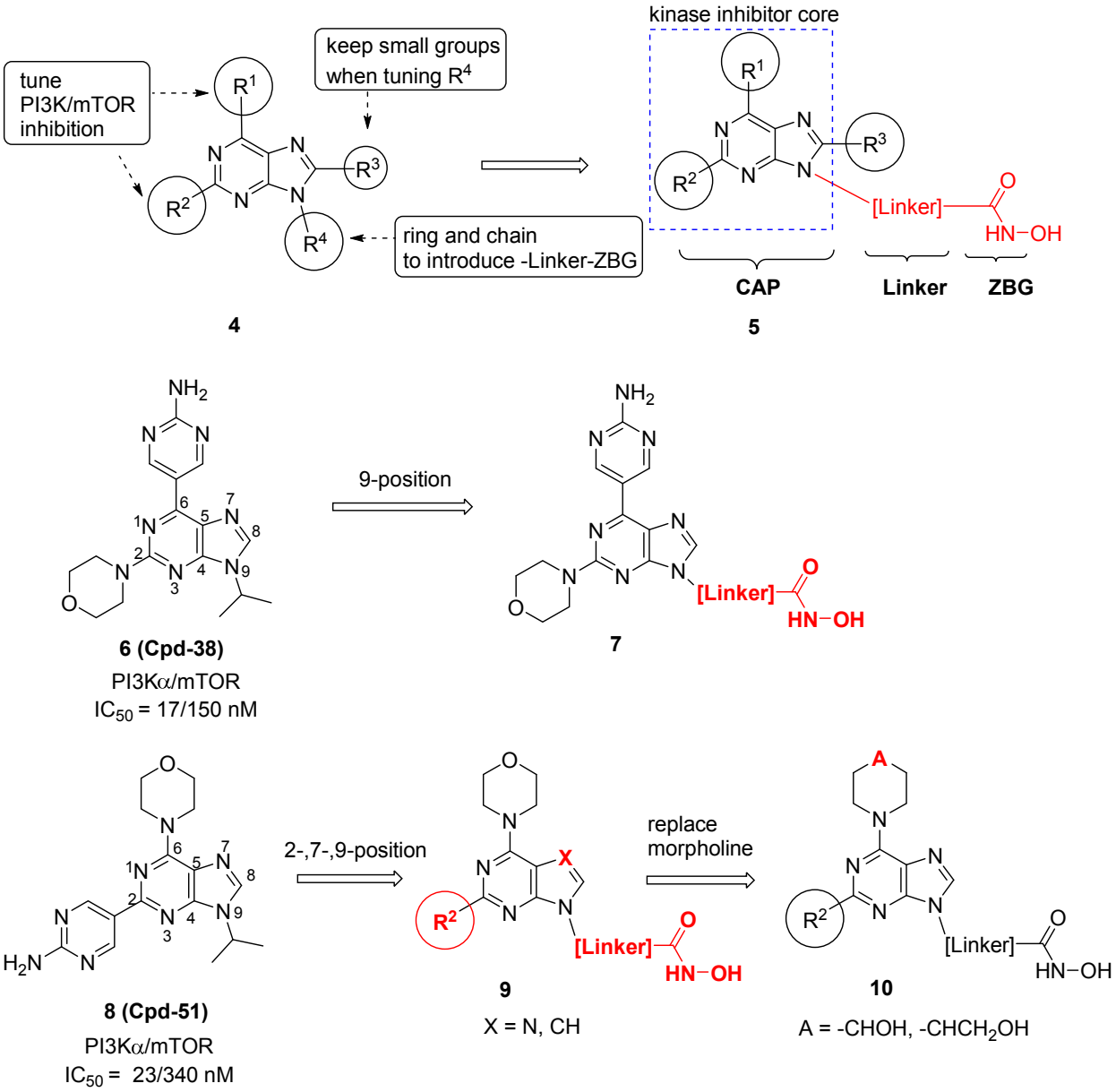

Figure 2. Design and chemical types of inhibitors targeting HDACs, PI3Ks and mTOR. IC_{50} data of Cpd-38 (**6**) and Cpd-51 (**8**) were extracted from ref 26.

RESULTS AND DISCUSSION

Chemistry. A wide range of substituted purines and pyrrolo[2,3-d]pyrimidines were prepared in a straightforward four- or five-step procedure starting from 2,6-dichloropurine (**11a**) or 2,4-

dichloro-7H-pyrrolo[2,3-d]pyrimidine (**11b**) which were commercially available. As depicted in Scheme 1, a typical procedure used an alkyl halide in the presence of a suitable base such as potassium carbonate to alkylate the NH group of compound **11a** or **11b**. The major products were N-9 alkylated **13a–d** when purine **11a** was used. The two chlorine atoms of **13a–d** were displaced selectively or sequentially under optimal reaction conditions. Under Suzuki reaction conditions, a boronic ester (**14a**) reacted with the more reactive chlorine atom to form mono-chloro compound **15a–d**. The 2nd chlorine atom was displaced by an amine (e.g., morpholine) at elevated temperature to give the esters **16a–d**, which were further converted to the hydroxamic acids **17a–d** by hydroxylaminolysis in the presence of excessive hydroxylamine.

Scheme 1. Synthesis of N-9 Substituted Purines 17a–d[a]

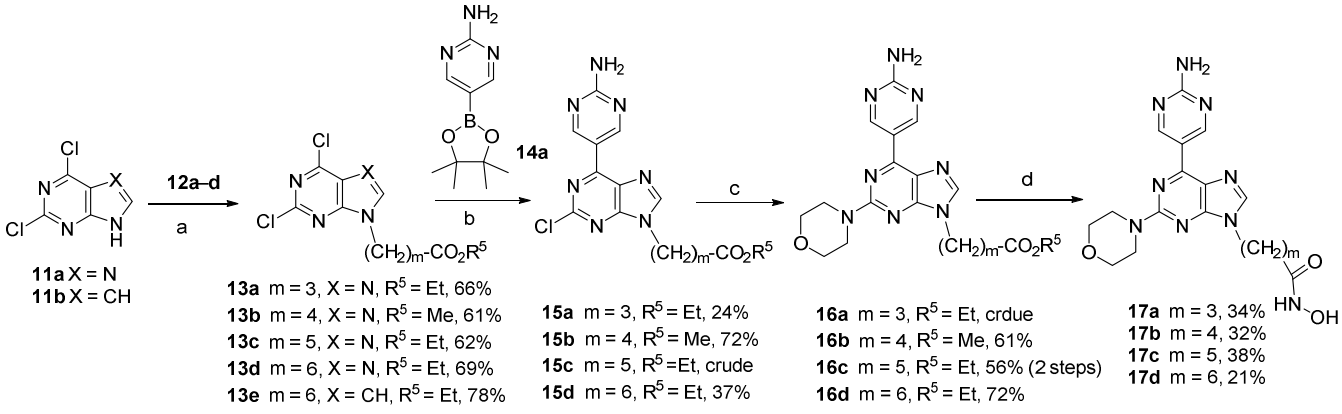

[a]Reagents and conditions: (a) NaI (0.2 equiv), anhydrous K_2CO_3 (2 equiv), $Br(CH_2)_mCO_2R^5$ (**12a–d**, m = 3,4,5,6; R^5 = Et or Me; 1.1 equiv), DMF, 40 °C, 12 h, 61–78%; (b) **14a** (1.1 equiv), K_2CO_3 (2.5 equiv), dioxane/water, $Pd(dppf)Cl_2 \cdot CH_2Cl_2$ (0.05 equiv), 82 °C for 6 h, 24–72%; (c) morpholine, DMF, 80 °C, 12 h, 56–72%; (d) $NH_2OH \cdot HCl$ (10 equiv)/NaOMe (25 equiv)/MeOH, −20 ºC to rt, 21–38%.

Table 1. SAR of N-9 Substituted Purines 17a–d

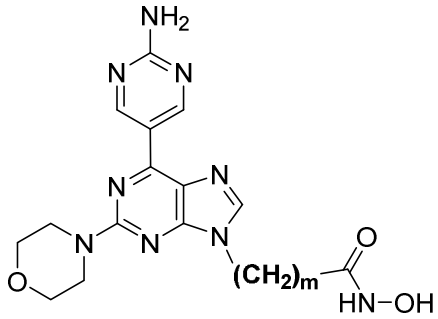

Compd	m	HDAC1[a] IC_{50} (nM)	PI3Kα[a] IC_{50} (nM)	MV4-11[b] IC_{50} (μM)	PC-3[b] IC_{50} (μM)	MCF7[b] IC_{50} (μM)
17a	3	>9257	12.8 ± 12.0	20.3 ± 2.5	>25	12.9 ± 1.9
17b	4	1754 ± 299	8.7 ± 4.6	9.81 ± 0.25	18.1 ± 6.1	11.1 ± 2.5
17c	5	60 ± 58	9.2 ± 6.3	2.81 ± 0.39	9.28 ± 3.03	7.37 ± 1.40
17d	6	17 ± 9	19.0 ± 0.1	0.25 ± 0.01	2.33 ± 0.46	2.08 ± 0.48
vorinostat		50 ± 30	NT	0.43 ± 0.10	3.07 ± 1.08	1.60 ± 0.31
wortmannin		NT	10.1 ± 7.1	NT	NT	NT
1		NT	7.8 ± 3.5	0.20 ± 0.03	0.18 ± 0.06	0.13 ± 0.05
pictilisib		NT	18.7 ± 8.6	1.46 ± 1.09	0.75 ± 0.36	0.22 ± 0.18

[a]Values are expressed as mean ± standard deviation (SD) of at least two independent experiments. [b]Values are expressed as mean ± SD of at least two independent duplicate experiments. NT: not tested.

Scheme 2 depicted an alternative displacement sequence of the two chlorine atoms of compounds **13c–e**. The more reactive chlorine was displaced first by morpholine to give **18c–e**, and the second chlorine was used to introduce aryl groups via Suzuki coupling by reaction with boronic acid or ester **14a–o** to afford esters **19a–t** which were subsequently converted to the hydroxamic acids **20a–s**. For those aryl groups could not directly derive from the readily

available **14a–o**, one additional step was applied to modify the analogues of **19a–t**. The reactive phenol group in **19t** or **19p** was alkylated by 2-bromoethanol and subsequently the resulting product **19t2** or **19u** was converted to **20t** or **20u**, which was extended with a neutral hydroxyl group. The aldehyde **19v** was reduced to the benzyl alcohol **19w**, which was subsequently converted to the final hydroxamate **20v**.

Scheme 2. Synthesis of 2-Aryl-9-Substituted Purines and Pyrrolo[2,3-d]pyrimidines 20a–v[a]

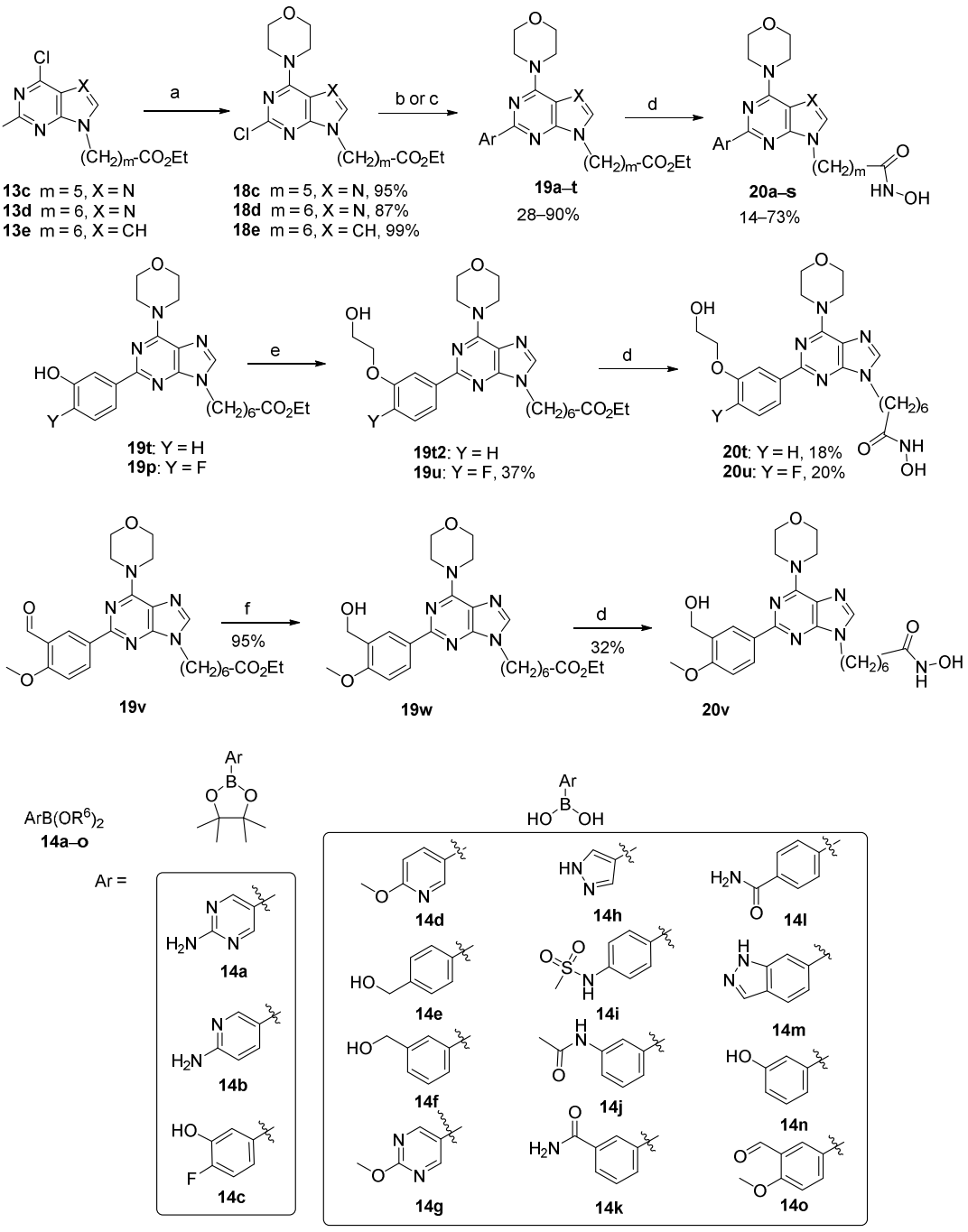

[a]Reagents and conditions: (a) morpholine (3 equiv), DCM, 40 °C, 3 h or rt overnight, 87–99%; (b) boronic acid or ester **14a-o** (1.1 equiv), K_2CO_3 (2.5 equiv), dioxane/water, $Pd(dppf)Cl_2 \cdot CH_2Cl_2$ (0.05 equiv), 82 °C for 6 h, 28–90%; (c) neat morpholine (excess), 78 °C,

overnight; (d) $NH_2OH \cdot HCl$ (10 equiv)/NaOMe (25 equiv)/MeOH, –20 ºC to rt; (e) 2-bromoethanol (3 equiv), K_2CO_3 (5 equiv), DMF, 90 °C; (f) $NaBH_4$ (10 equiv), MeOH, rt, 95%.

Scheme 3 depicted another modification: replacing the commonly used morpholine at the 6-positon of the purine ring with other cyclic amines. Both piperidin-4-ylmethanol and piperidin-4-ol were used to react with **13d** to afford **21a** and **21b**, which were further converted to hydroxamates **23a** and **23b** via Suzuki coupling and hydroxylaminolysis.

Scheme 3. Synthesis of 6-Substituted Purines 23a and 23b[a]

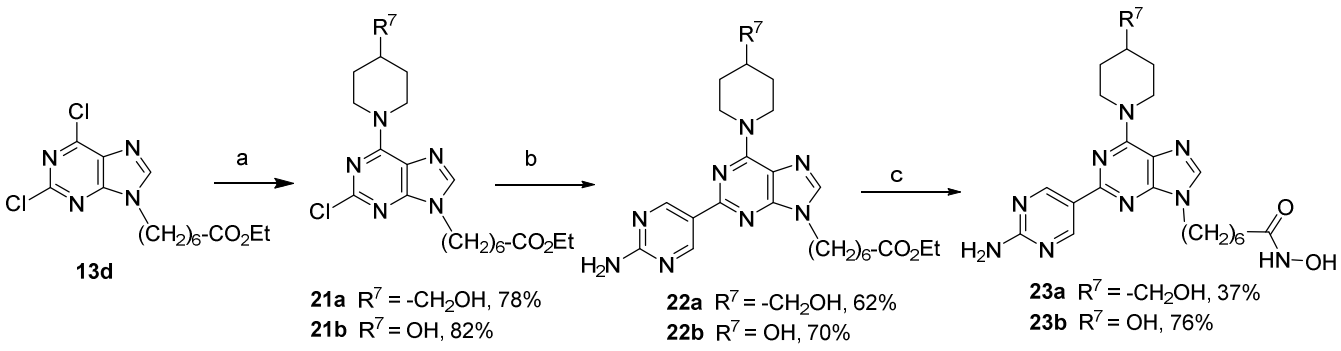

[a]Reagents and conditions: (a) **13d** (1 equiv), piperidin-4-ylmethanol or piperidin-4-ol (6 equiv), Et_3N (6 equiv), DCM, 40 °C, overnight; (b) **14a** (3 equiv), K_2CO_3 (4 equiv), dioxane/water, $Pd(dppf)Cl_2 \cdot CH_2Cl_2$ (0.05 equiv), microwave 150 °C, 10–30 min; (c) $NH_2OH \cdot HCl$ (10 equiv)/NaOMe (25 equiv)/MeOH, –20 ºC to rt.

Table 2. SAR of 2-Aryl-9-Substituted Purines and Pyrrolo[2,3-d]pyrimidines 20a–v

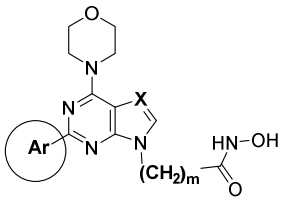

Compd	Ar	X	m	HDAC1[a] IC_{50} (nM)	PI3Kα[a] IC_{50} (nM)	MV4-11[b] IC_{50} (μM)	PC-3[b] IC_{50} (μM)
20a	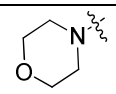	N	6	5.55 ± 0.38	>10,000	0.78 ± 0.05	3.60 ± 0.90
20b	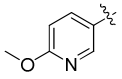	N	5	12 ± 2	724 ± 156	6.84 ± 2.66	17.4 ± 1.5
20c	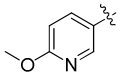	N	6	2.9 ± 1.2	>1000	1.99 ± 0.12	8.48 ± 0.32
20d	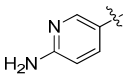	N	5	35 ± 8	>10,000	2.39 ± 1.81	6.97 ± 1.23
20e	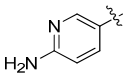	N	6	0.85 ± 0.34	196±26	0.045 ± 0.036	4.01 ± 1.43
20f	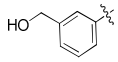	N	6	2.7 ± 1.2	50 ± 5	0.047 ± 0.030	1.08 ± 0.82
20g	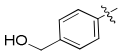	N	6	4.4 ± 5.4	>1000	0.08 ± 0.09	3.64 ± 1.03
20h	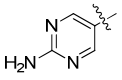	N	6	2.3 ± 1.8	38 ± 27	0.034 ± 0.015	2.26 ± 0.63
20i	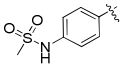	N	6	1.2 ± 0.8	>1000	0.061 ± 0.006	6.04 ± 1.19
20j	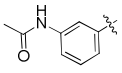	N	6	0.78 ± 0.02	>863	0.058 ± 0.003	3.53 ± 0.31
20k	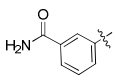	N	6	0.84 ± 0.29	>924	0.059 ± 0.004	3.47 ± 0.16

Compd	Ar	X	m	HDAC1[a] IC_{50} (nM)	PI3Kα[a] IC_{50} (nM)	MV4-11[b] IC_{50} (μM)	PC-3[b] IC_{50} (μM)
20l	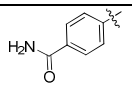	N	6	0.61 ± 0.06	>1000	0.017 ± 0.002	3.02 ± 0.33
20m	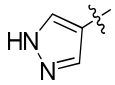	N	6	1.7 ± 1.0	>1000	0.31 ± 0.04	2.81 ± 0.16
20n	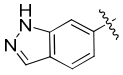	N	6	1.4 ± 0.1	>6663	1.36 ± 0.51	7.54 ± 0.15
20o	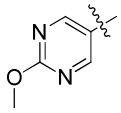	N	6	2.7 ± 0.4	376	0.062 ± 0.026	2.77 ± 1.00
20p	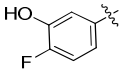	N	6	0.49 ± 0.21	619 ± 16	1.81 ± 0.16	5.67 ± 1.03
20q	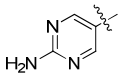	CH	6	1.5 ± 0.5	25 ± 10	0.044 ± 0.027	1.57 ± 0.69
20r	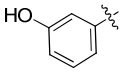	CH	6	1.6 ± 0.3	41 ± 8	0.13 ± 0.01	1.70 ± 0.57
20s	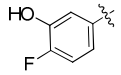	N	5	8.5 ± 2.5	317 ± 23	7.39±0.41	17.2 ± 2.8
20t	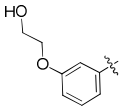	N	6	0.76 ± 0.65	994 ± 22	0.030 ± 0.008	1.68 ± 1.12
20u	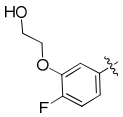	N	6	3.7 ± 1.4	6439 ± 180	1.88 ± 0.14	4.69 ± 0.70
20v	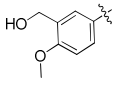	N	6	0.89 ± 0.41	218 ± 14	0.38 ± 0.06	2.00 ± 0.17
1				NT	7.8 ± 3.5	0.20 ± 0.03	0.18 ± 0.06
pictilisib				NT	18.7 ± 8.6	1.46 ± 1.09	0.75 ± 0.36
vorinostat				50 ± 30	NT	0.43 ± 0.10	3.07 ± 1.08

Compd	Ar	X	m	HDAC1[a] IC_{50} (nM)	PI3Kα[a] IC_{50} (nM)	MV4-11[b] IC_{50} (μM)	PC-3[b] IC_{50} (μM)
wortmannin				NT	10.1 ± 7.1	NT	NT

[a,b] See footnote of Table 1.

Table 3. SAR of 6-Substitutedamino Purines 23a and 23b

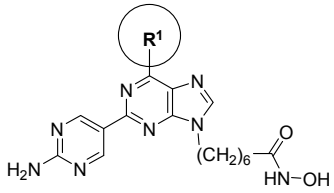

Compd	R^1	HDAC1[a] IC_{50} (nM)	PI3Kα[a] IC_{50} (nM)	MV4-11[b] IC_{50} (μM)	PC-3[b] IC_{50} (μM)	MCF7[b] IC_{50} (μM)
23a	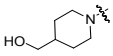	0.99 ± 0.35	1041 ± 203	0.17 ± 0.05	1.94 ± 0.19	2.56 ± 1.58
23b	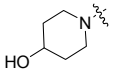	0.69 ± 0.10	3955 ± 1688	0.13 ± 0.03	1.68 ± 0.74	1.21 ± 0.48
20h	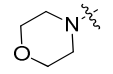	2.3 ± 1.8	38 ± 27	0.034 ± 0.015	2.26 ± 0.63	0.95 ± 0.69

[a,b] See footnote of Table 1.

Scheme 4 depicted the approaches to introduce aryl linked hydroxamates at the 9-position of the purine ring. The more reactive 6-Cl of **11a** was first replaced with morpholine, and then the resulting 6-morpholinopurine **24** was subjected to further alkylation. This approach was also applied to make individual compounds described in both Schemes 2 and 3. Nitrile **25** was prepared by N-9 alkylation of **24** with 2-iodoacetonitrile and was further reduced to amine **26**.

By reductive amination with aldehyde and alkylation with alkyl bromide, amine **26** was converted to intermediates **27** and **32** with aryl linkers, respectively. After Suzuki coupling with either boronic ester **14a** or boronic acid **14d**, and subsequent hydroxylaminolysis, **27** and **32** were eventually converted to hydroxamates **29**, **31** and **34**.

Table 4. **SAR of N-9 Aryl linked Purine Hydroxamates 29, 31 and 34**

Compd	HDAC1[a] IC_{50} (nM)	PI3Kα[a] IC_{50} (nM)	MV4-11[b] IC_{50} (μM)	PC-3[b] IC_{50} (μM)
29	84 ± 40	>8956	0.24 ± 0.07	1.72 ± 0.81
31	136 ± 10	307 ± 57	5.44 ± 1.73	>25
34	1082 ± 192	4543 ± 1136	5.78 ± 0.64	18.5 ± 6.3

[a,b] See footnote of Table 1.

The acid (RCO_2H) was identified as the major impurity in the final target hydroxamate (RCONHOH) product. In general, the hydroxamic acid was slightly more polar than the acid and was separated by preparative HPLC with purity >95%. The acid (**20w**) corresponding to **20f** was prepared by hydrolysis of the ester **19f** (Supporting Information), was a very poor HDAC inhibitor as compared to the respective hydroxamic acid **20f**, it still maintained majority of the PI3K inhibitory potency, but its contribution to biological activity was insignificant or negligible (**20f** vs **20w**, Table S1).

Scheme 4. Synthesis of N-9 Aryl linked Purine Hydroxamates 29, 31, and 34[a]

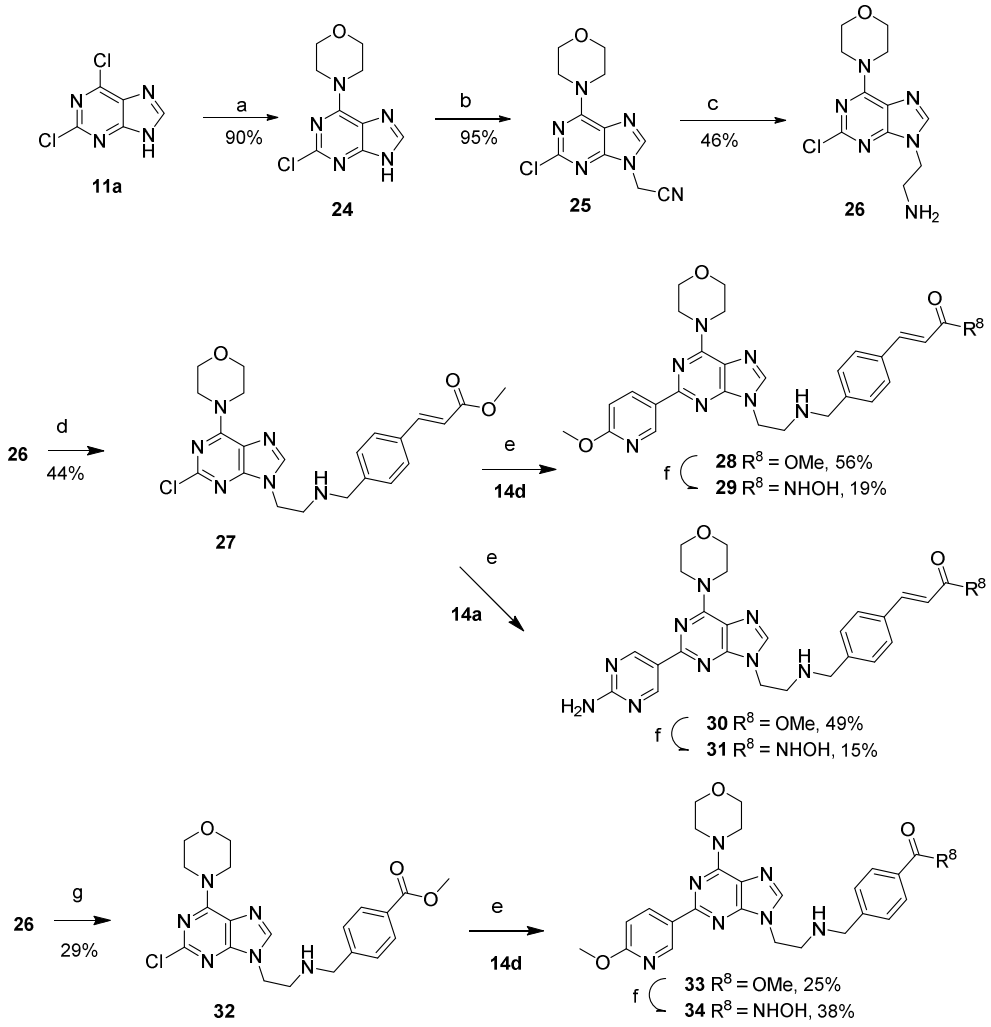

[a]Reagents and conditions: (a) morpholine (3 equiv), rt, THF; (b) ICH_2CN (2 equiv), anhydrous K_2CO_3 (2 equiv), MeCN-DMSO (19:1, v/v), 60 ºC; (c) $NiCl_2 \cdot 6H_2O$ (0.1 equiv), $NaBH_4$ (7 equiv), THF/MeOH (1:2); (d) methyl 3-(4-formylphenyl)acrylate (1.2 equiv), $NaBH(OAc)_3$ (1.5 equiv), HOAc (1 equiv), DCE, rt; (e) **14a** or **14d** (2.0 equiv, Scheme 2), K_2CO_3 (2.0 equiv), dioxane/water, $Pd(dppf)Cl_2 \cdot CH_2Cl_2$ (0.05 equiv), microwave 15–30 min; (f) $NH_2OH \cdot HCl$ (10 equiv)/NaOMe (25 equiv)/MeOH, −20 ºC to rt; (g) *p*-$BrCH_2C_6H_4CO_2CH_3$ (1.1 equiv), Et_3N (1.2 equiv), THF, rt, 2 h.

Inhibition of HDAC1 and PI3Kα, SAR and Anti-proliferative Activity. HeLa nuclear extract and HDAC isozyme HDAC1 as well as PI3Kα (p110α/p85α) were used as routine enzymatic screening tests for HDAC and PI3K inhibitory activities. Cancer cell lines MV4-11

(acute monocytic leukemia), PC-3 (prostate cancer) and MCF7 (breast cancer) were used to evaluate anti-proliferative activities as well as modulation of targets (HDACs, PI3K, mTOR) in cancer cells. HDAC inhibitor vorinostat and PI3K inhibitor pictilisib were used as positive control in all experiments.

To establish SAR, we tried to optimize HDAC inhibitory activity first and started from a PI3K inhibitor core structure with fixed functional groups which were good for PI3K inhibition. According to our previous study, purine-based PI3K/mTOR inhibitor **1** (Figure 1) or **4** (Figure 2), the 2-aminopyrimidin-5-yl group was good for PI3Kα and mTOR inhibition (e.g., **6** and **8**), and 9-position could accommodate substituents such as rings or chains of reasonable size, [26] and thus a batch of compounds **17a–d** (Table 1) were first synthesized. Their PI3Kα inhibitory IC_{50} values were comparable to that of **1**, however their HDAC IC_{50} values were correlated with the length of carbon linker. It was found that C6 (six methylenes) or six atoms linker was optimal; these results were in line with the previous reported SAR for acylurea linked hydroxamates. [23] The anti-proliferative potencies were also improved along with the linker length, but even the best compound **17d** which showed better HDAC inhibitory potency than vorinostat was less potent than vorinostat in cells. Besides target potency, the physicochemical properties may also affect cellular potency. Polar group 2-aminopyrimidin-5-yl at 1-position and linker-hydroxamic acid at 9-position of the purine molecule may not be the best arrangement. Next we tried to swap the morpholine and 2-aminopyrimidine groups to create molecules like **8** or **9** (Figure 2). A series of compounds **20a–v** were thus made to further confirm the optimal linker for HDAC inhibition and explore PI3K/mTOR inhibitory potency SAR (Table 2).

The C6 linker for hydroxamate was still preferred (**20b** vs **20c**, **20d** vs **20e**, and **20s** vs **20p**), and the HDAC1 IC_{50} value went down to 1 nM, this was still valid for most of the compounds

with C6 linker in Table 2. The IC_{50} value didn't change significantly with a variety of substituents at 2-position of the purine nor pyrrolo[2,3-d]pyrimidine ring, as these lipophilic purines or pyrrolo[2,3-d]pyrimidines were excellent CAPs for HDAC inhibitors. Therefore there was leeway to tune PI3K/mTOR inhibitory potency in these SARs. 2-Aminopyrimidin-5-yl group was still one of the best groups for PI3K inhibition (e.g., **20h** and **20q**), metabolically labile *meta* phenol group was also good (**20r**) for PI3Kα inhibition (similar to **2**), and *meta* benzyl alcohol (**20f**) was found to be a good replacement of the phenol and demonstrated comparable PI3Kα potency. The binding site cannot tolerate big or bulky groups as we reported earlier,[26] such compounds (**20i–l**, **20n**, **20t**, and **20u**) didn't show any appreciable potency against PI3Kα. Adding *para* substituent to *meta* phenol (**20p** and **20s**) or benzyl alcohol (**20v**) actually reduced the PI3Kα potency. Compound **20g** with *para* benzyl alcohol group was no longer active against PI3Kα. Compounds **20f**, **20h**, **20q**, **20e**, and **20o** were very potent HDAC inhibitors with variable PI3Kα potency and showed good cellular activates as well, were worth of further profiling and evaluation.

Morpholine ring was commonly used in PI3K inhibitors, [40] it also showed good activity at purine 6-position in above mentioned series. A few substituents were tried to replace the morpholine, such as **23a** and **23b**, unfortunately they significantly destroyed PI3Kα affinity, but still kept the HDAC inhibitory effect intact.

Besides aliphatic linkers, aryl linker was also commonly used for HDAC inhibitors. We made several compounds with aryl linker at N-9 position to investigate the HDAC potency. Both **29** and **31** with cinnamic linkers showed moderate HDAC potency, but the PI3Kα potency was affected even with the best 2-aminopyrimidine group, the N-9 substituent was too big and basic

(secondary amine). **34** was linked with a shorter benzylamine linker unit and showed even poorer HDAC inhibitory potency.

Molecular Docking Study. To better understand the above observed SAR for PI3Kα inhibition, molecular docking study was performed using AutoDock Vina software[41] and crystal structure of PI3Kα–**3** complex (PDB ID code: 4L23)[42] (Supporting Information, Figure S2). For these morpholino-pyrimidine based PI3K inhibitors, there are two major binding modes. One is represented by **2** (Figure S2A and Figure S2B), and the other is represented by **1** (Figure S2D). The backbone NH group of Val851 in the hinge region is a hydrogen bond donor, it forms a hydrogen bond with the 1-position nitrogen atom of the ATP purine ring, and this interaction is critical to kinase activity. The oxygen of the morpholine group of **2** is a hydrogen bond acceptor and forms a hydrogen bond with the NH group of Val851 (Figure S2B). Forming this bond enables **2** to compete with ATP in the ATP binding pocket. The hydroxyl group of the phenol ring of **2** also forms another two key hydrogen bonds with the residues of Tyr836 and Asp810. Compound **10r**, which has a *meta* phenol group as well, shows a similar binding mode (Figure S2E). **20p** has similar interactions with the key residues, but the inhibitory potency is lower, probably due to the unfavorable interaction between the fluorine atom and the hydroxyl group (Figure S2F). The *meta* benzyl alcohol group of **20f** interacts with the residues of Asp810, Tyr836 and Asp933 (Figure S2G), which makes **20f** a potent PI3Kα inhibitor. In contrast, the *para* benzyl alcohol group of **20g** is far away from Tyr836, and only forms a hydrogen bond with Asp810. Furthermore, the oxygen of benzyl alcohol group is unfavorably close to the carboxylic group of Asp933 (Figure S2H). This is why **20g** loses PI3Kα inhibitory activity dramatically as compared to **20f** (Figure S2I). Pictilisib does not have a hydroxyl group, but its 1H-indazol-4-yl group forms two hydrogen bonds with Tyr836 and Asp810 (Figure S2C), and therefore it is also

a potent PI3Kα inhibitor. Compound **20n** also has an indazole group, but it is 1H-indazol-6-yl and thus only forms a hydrogen bond with Asp810 (Figure S2J). The hydrogen bond with Tyr836 is very important in achieving a ligand's inhibitory activity, for example, an Y836A mutation resulted in 44-fold reduction of **2**'s potency against PI3Kα.[42]

Compound **1** represents the second binding mode, its *para* amino group of the 2-aminopyrimidine group forms two hydrogen bonds with Asp810 and Asp933, and the two nitrogen atoms in the pyrimidine ring form additional hydrogen bonds, one with Lys802, and the other with the NH group of Asp933 or hydroxyl group of Tyr836 (Figure S2D). Compounds **17d** (Figure S2K), **20h** (Figure S2L) and **20q** (Figure S2M) all have 2-aminopyrimidine groups: they show similar binding mode as that of **1** and are also potent PI3Kα inhibitors. **20e** has an amino-pyridine group and it forms fewer hydrogen bonds as compared to 2-aminopyrimidine group (Figure S2N), therefore its potency is lower than **20h** or **20q**. **23a** (Figure S2O) and **23b** (Figure S2P) are two analogues of **20h**, with the morpholine group being replaced by piperidines. In order to make similar contact with Val851, the hydroxyl group repels the entire molecule away from the binding pocket (i.e., Trp780, Met772, Met922, Ile800, Ile932, Tyr836 and Asp933), but pushes it slightly closer to Lys802 as compared to **20h**. Furthermore, the piperidine has to adopt a conformation notably different from that of the morpholine in **20h**. In contrast, all rings including the morpholine of **20h** superpose well on **2** (Figure S2L). Hence, **23a** and **23b** are poor PI3Kα inhibitors. Interestingly, **23a** is about 4-fold as potent as **23b**. Its flexible primary alcohol may allow it to adopt a more favorable conformation in order to form a hydrogen bond with the NH group of Val851 in contrast to that of the rigid secondary alcohol in **23b**. It is thus clear that piperidine is not a suitable replacement for the morpholine group in the current chemical series.

In Vitro Profiling against HDACs and Kinases. Besides in house assays, the HDAC isoform profiling was done at BPS Bioscience. In additional to routine controls such as vorinostat and trichostatin A (TSA), **3** and pracinostat were also included for comparison. The data for **3**, except for class IV HDAC11, were generally in line with reported data generated with different substrate.[36] IC_{50} values of pracinostat were also in line with the trend of our previous reported Ki values which were derived from IC_{50} values, except for HDACs 4, 5, 7, 8 and 11 which were tested using class 2a substrate. **20e**, **20f** and **20q** were potent nanomolar inhibitors for HDACs 1, 2, 3, 6, and 10, but poor inhibitors for classes IIa and IV HDACs.

Selected compounds **20f** and **20q** were also profiled against a panel of 97 kinases: both were found selective against lipid kinases (Supporting Information Table S2), and their K_d values were determined (Table 6). The PI3K and mTOR inhibitory IC_{50} values were determined at both Reaction Biology Corp and Life Technologies, the data agreed well from two different assay platforms. Additional kinase profiling was done at Life Technologies with **3** as positive control. Pictilisib was the most potent PI3K inhibitor, but a poor mTOR inhibitor. **3** showed reasonable potency against mTOR, and was still a pan-inhibitor for PI3K. Compounds **20h**, **20e** and **20q** were active against mTOR, **20f** was a weaker mTOR inhibitor thus more selective for PI3K, was also potent against PI3K2β, which was confirmed by two different assay platforms.

Compounds **20f**, **20h**, **20e**, **20o**, and **20q** achieved dual or multi inhibitions of HDACs and PI3K/mTOR. They were very potent pan-HDAC inhibitors with a different degree of inhibitory potency against PI3K/mTOR, thus were good examples for further evaluation in order to identify the optimal combination of HDAC and PI3K/mTOR.

Table 5. Inhibition of HDAC Isozymes by Selected Compounds

	IC_{50} (nM) for HDAC Isozymes[a]										
Compd	1	2	3	4	5	6	7	8	9	10	11
20e	1.0	4.0	2.0	>10,000	>10,000	4.6	>10,000	184	>10,000	1.7	>10,000
20f	1.1	6.0	1.1	4,591	4,800	4.2	2,305	320	1,282	2.5	9,700
20q	1.5	4.1	0.66	>10,000	>10,000	6.6	>10,000	270	>10,000	2.3	6,300
vorinostat	81	220	34	NT	NT	12	NT	NT	NT	27	NT
TSA	NT	NT	NT	NT	NT	NT	NT	490	NT	NT	10,900
pracinostat	50	290	70	>10,000	5,113	93	>10,000	2,835	>10,000	82	>10,000
3	2.0	8.0	3.2	479	581	34	528	54	639	4.1	1,267

[a]HDAC profiling was done by BPS Bioscience (6042 Cornerstone Court West, Suite B, San Diego, CA 92121), HDAC Substrate 3 (BPS catalog #50037) was used for class I HDACs (HDACs 1, 2, and 3) and class IIb HDACs (HDACs 6 and 10) and vorinostat as positive control; substrate class 2a (catalog # 50040) was used for class IIa HDACs (HDACs 4, 5, 7, and 9) as well as HDACs 8 (class I) and 11 (class IV), using TSA as positive control. TSA: trichostatin A. NT: not tested.

Table 6. Inhibition of Lipid and Relevant Kinases by Selected Compounds

	K_d (nM)[a]		IC_{50} (nM)[b]							
Kinases	**20f**	**20q**	**20h**	**20e**	**20f**	**20o**	**20q**	Pictilisib	**3**	**2**
PI3Kα	3.5	12	29	198	28	136	11	4.7	7.9	3.8
PI3Kβ	NT	NT	648	1656	212	1403	87	NT	21	10
PI3Kγ	86	100	98	793	177	692	92	NT	112	71
PI3Kδ	41	240	133	301	37	331	63	NT	6.3	11
mTOR	NT	NT	288	374	1,946	4,945	101	959	185	141
PI3K2α	NT	NT	>1,000	>10,000	>1,000	>10, 000	>1,000	NT	NT	NT
PI3K2β	4.9	260	>1,000	>1,000	103	>1,000	1,046	NT	NT	NT
DNA-PK	NT	NT	>1,000	>10,000	10,000	>10,000	594	NT	3,673	NT
PIK3C3	NT	NT	>10,000	>10,000	10,000	>10,000	6,295	NT	>10,000	NT
PI4Kβ	NT	NT	>10,000	>10,000	>10,000	>10,000	>10,000	NT	NT	NT

[a] K_d values were determined by DiscoverX Corporation (42501 Albrae Street, Fremont, CA 94538, United States). [b] PI3K and mTOR IC_{50} values were determined by Reaction Biology Corp. (One Great Valley Parkway Suite 2, Malvern, PA 19355, United States) and Life Technologies. NT: not tested.

Table 7. Anti-Proliferative IC_{50} (μM) of Selected Compounds[a]

Cancer	Cell Lines	**20e**	**20f**	**20q**	Pictilisib	Vorinostat	Sorafenib
Leukemia	K562	0.60 ± 0.30	0.35 ± 0.14	0.44 ± 0.32	6.34 ± 3.09	1.02 ± 0.12	5.08 ± 0.37
	MOLT4	0.16 ± 0.10	0.14 ± 0.11	0.15 ± 0.07	0.18 ± 0.04	0.52 ± 0.16	5.94 ± 0.04
	MV4-11	0.045 ± 0.036	0.047 ± 0.030	0.044 ± 0.027	1.46 ± 1.09	0.43 ± 0.10	<0.006
Lymphomas	Raji	0.35 ± 0.15	0.24 ± 0.04	0.28 ± 0.08	6.50 ± 3.23	1.11 ± 0.48	3.94 ± 0.04
	Ramos	0.60 ± 0.18	0.40 ± 0.13	0.49 ± 0.18	4.86 ± 1.79	0.62 ± 0.07	NT
	SU-DHL-6	0.23 ± 0.12	0.19 ± 0.06	0.25 ± 0.14	0.03 ± 0.01	0.58 ± 0.17	3.82 ± 0.02
Liver cancer	Hep3B	1.55 ± 0.15	1.25 ± 0.20	2.87 ± 0.26	2.03 ± 1.02	2.60 ± 0.56	4.33 ± 1.16
	HepG2	0.96 ± 0.29	0.59 ± 0.11	1.05 ± 0.25	6.22 ± 1.83	1.27 ± 0.10	3.66 ± 0.90
	HuH-7	0.50 ± 0.19	0.48 ± 0.13	0.65 ± 0.20	1.72 ± 0.02	1.95 ± 0.39	2.68 ± 0.28
	PLC/PRF/5	1.57 ± 0.24	1.24 ± 0.08	3.05 ± 0.41	3.07 ± 0.74	1.87 ± 0.16	7.51 ± 2.59
	SK-HEP1	1.16 ± 0.23	0.79 ± 0.20	1.46 ± 0.54	4.30 ± 0.24	1.85 ± 0.28	8.37 ± 3.84
	SNU-387	3.15 ± 2.16	2.64 ± 1.50	3.90 ± 0.79	NT	2.45 ± 0.69	8.29 ± 0.75
	SNU-398	1.52 ± 0.63	1.38 ± 0.57	1.66 ± 0.54	NT	1.39 ± 0.31	3.38 ± 0.43

[a]Values are expressed as mean ± SD of at least two independent duplicate experiments. NT: not tested.

In Vitro Anti-proliferation Profiling. Lead compounds were screened against 39 cancer cell lines (Supporting Information Table S3) in anti-proliferative assays (cellular IC_{50}) and were found more sensitive/potent against leukemia, lymphoma and HCC cell lines (Table 7). For instance, **20e**, **20f** and **20q** were very active against leukemia cell line MV4-11, and were much more potent than pictilisib and vorinostat. Sorafenib in general was much less potent than these compounds as its mechanism is mainly anti-angiogenesis in vivo. Sorafenib's exceptional activity against MV4-11 might be due to its inhibition of multi-kinase particularly FLT3. Among liver cancer cell lines, **20f** was more potent against HepG2, HuH-7 and SK-HEP1.

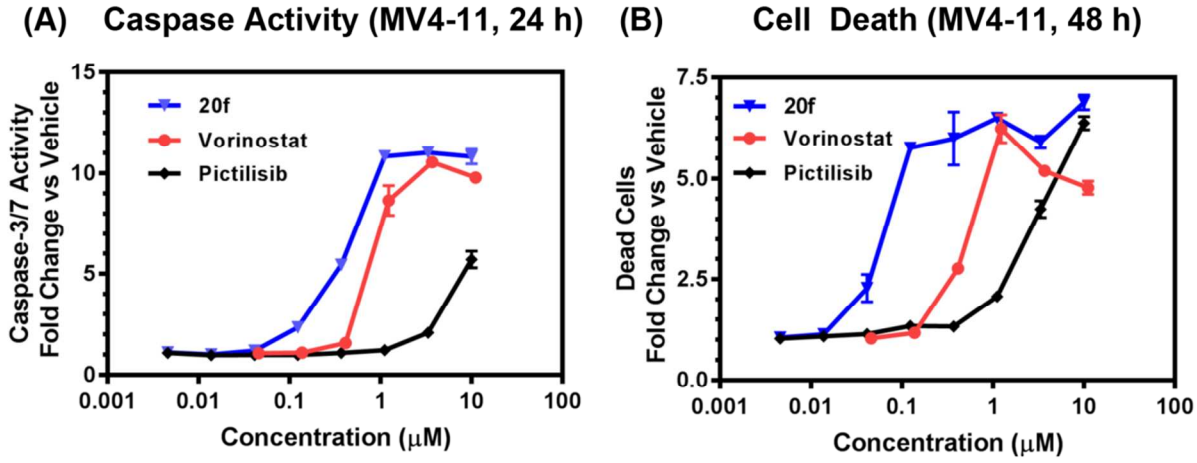

Figure 3. Caspase activity induction and cell death in MV4-11 cells. (A) Maximal caspase activity at 24 h. MV4-11 cells were treated with **20f** (▼), vorinostat (●), and pictilisib (♦), respectively. Caspase 3/7 activity was monitored at 6, 24, 48 and 72 h, respectively. Maximal activity was found and shown at 24 h, expressed as fold of change (treated vs vehicle, mean ± SD). (B) Maximal cell death occurred at 48 h. MV4-11 cells were treated with **20f** (▼) vorinostat (●), and pictilisib (♦), respectively. Cell death was monitored at 24, 48 and 72 h Maximal cell death as fold of treated vs vehicle was occurred at 48 h. Y Axis is expressed as mean ± SD. EC_{50} value was calculated by fitting the dose-response curve with Prism 4.0.

Caspase Activity Induction and Cell Death. HDAC inhibitors can induce cell apoptosis[43] Caspase-3/7 activity was used as a surrogate for apoptotic cell death induction. Cells were treated with **20f**, vorinostat and pictilisib, respectively and caspase activity was monitored at different time points. The maximal activity was found and shown at 24 h. The caspase induction effective concentrations (EC_{50}) were 0.40, 0.90, and 10.7 μM for **20f**, vorinostat and pictilisib, respectively. Maximal cell death as fold of treated vs vehicle was occurred at 48 h, the cell death potency EC_{50} was estimated as 0.064, 0.53 and 2.71 μM for **20f**, vorinostat and pictilisib, respectively. **20f** was much more potent than vorinostat and pictilisib in terms in induction of caspase active and cell death in MV4-11 cells.

Clonogenic and Soft Agar Assays. Anchorage-dependent clonogenic assay was used to determine cell reproductive death after treatment with **20f**. Liver cancer cells Hep3B and HuH-7 after treatment with a series dilution of **20f**, showed IC_{50} values of 0.61 μM and 0.39 μM, respectively, and these values were lower than their respective in vitro cellular assay IC_{50} values of 1.25 μM and 0.48 μM, respectively (Table 7). One of the hallmark characteristics of cellular transformation and uncontrolled cell growth is anchorage independent growth of cancer cells in soft agar. When **20f** was tested in a 3-dimensional (3D) soft agar format, it inhibited colony formation of NCI-H460 and 4T1 cells with IC_{50} values of 0.31 μM and 0.91 μM, respectively. Again these IC_{50} values were lower than the normal in vitro cellular assay IC_{50} values (0.89 μM and 1.29 μM for NCI-H460 and 4T1, respectively). These data suggested that **20f** could inhibit a variety of cancer cells under both anchorage-dependent and anchorage-independent conditions.

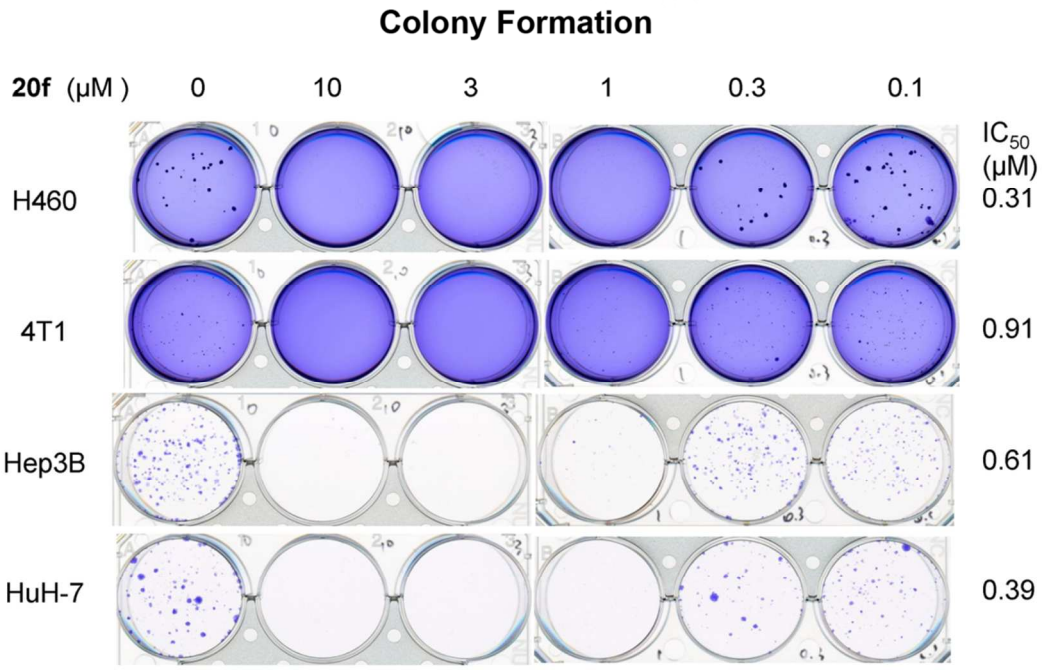

Figure 4. Clonogenic and soft agar assays and IC_{50} values. **20f** inhibited colony formation of Hep3B and HuH-7 cells under anchorage-dependent conditions and inhibited colony formation of NCI-H460 and 4T1 (murine triple negative breast cancer) cells in soft agar assays.

Modulation of HDACs and PI3K/mTOR in Cancer Cells and Tumors. Inhibition of HDACs will result in hyperacetylation of histones and other substrates such as α-tubulin, and the latter is the result of inhibition of HDAC6. Inhibition of PI3K/Akt/mTOR axis may reduce the phosphorylated Akt level as well as the phosphorylation levels of downstream proteins such as P70S6K, S6, and 4-EBP1. The effect on target modulation was first studied in PC-3 (PTEN deficient) and MCF7 (PIK3CA, E545K mutation) cells and most of the compounds were screened for target modulation.

In PC-3 cells, after 24 h of drug treatment, **20f**, **20g**, and **20h** were confirmed to be potent HDAC inhibitors as their effects on hyperacetylation of histone 3 (AcH3) and α-tubulin were

similar to those of vorinostat at 10 μM (Supporting Information Figure S1A). **17d** was a much weaker HDAC inhibitor as compared to **20f–h** in terms of enzymatic potency and cellular target modulation. Pictilisib was a very potent PI3K inhibitor and a weak mTOR inhibitor, it almost completely depleted pAkt at 1 μM. The order of potency in PC-3 cells for pAkt reduction was pictilisib > **20f** > **17d** > **20h** > **20g**. Vorinostat showed no effect on pAkt level in this experiment. In MCF7 cells, **20q** appeared as a potent effector on pAkt and pS6 reduction, as it was more potent than **20f** and also an mTOR inhibitor (Supporting Information Figure S1B). During the short period of time of treatment, these compounds didn't change the total protein levels in MCF7 cells (e.g., α-tubulin, Akt, P70S6K, and S6).

In liver cancer HepG2 cells, **20f** and **20q** were potent HDAC inhibitors in terms of hyperacetylation of H3 and α-tubulin (Figure 5A), while **3** was a weaker inhibitor on HDAC6. Acid **20w** is a potential impurity or degradation product of **20f**, still maintained the majority of PI3K inhibitory activity, but it showed much weak activity against HDAC6 and HDACs 1, 2, 3 in HepG2 cells. In HuH-7 cells (Figure 5B), the overall effect on phosphorylated Akt, P70S6K, and S6 was in the order of **20q** > **20f** > **20e** > **20o**, which was in line with their respective in vitro enzymatic IC_{50} potency against PI3Kα and mTOR. Sorafenib reduced pAkt level (gel normalized intensity 42% vs vehicle) at lower concentration (1 μM), but enhanced pAkt (S473) level (252% vs vehicle) at higher concentration (10 μM). These data further support that a PI3K/mTOR inhibitor is necessary to combine with sorafenib to reduce pAkt level.[13, 44, 45]

(A) Target Modulation in HepG2 Cells

Veh	Veh	Veh	20f	20f	20w	20q	3	Veh	20f	20f	20w	20q	3	Sample
-	-	-	10	1	30	1	1	0	10	1	30	1	1	Conc. (μM)
-	+	-	-	-	-	-	-	-	-	-	-	-	-	FGF2
-	-	+	+	+	+	+	+	-	-	-	-	-	-	IGF-1
-	-	-	-	-	-	-	-	+	+	+	+	+	+	EGF

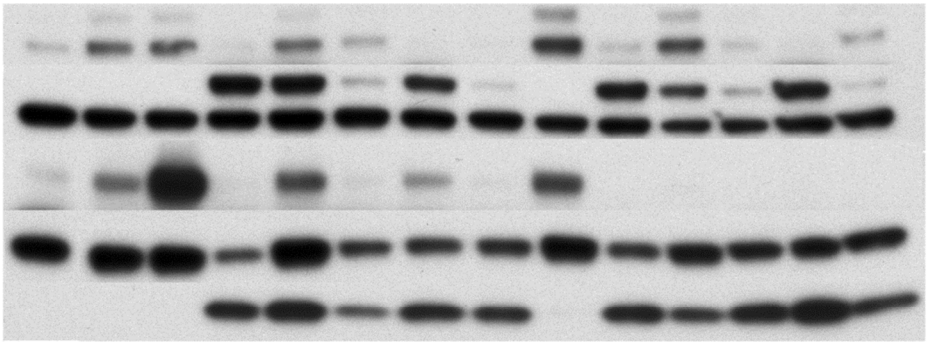

0.03	0.08	0.27	85	**100**	43	92	92	2.1	95	**100**	103	129	95	**AcH3 (%)**
0.00	0.00	0.00	114	**100**	12	79	4.7	0.16	132	**100**	28	135	10	**Ac-α-Tub (%)**
3.7	33	**100**	3.3	37	1.7	16	1.8	**100**	0.24	1.7	0.34	0.11	0.12	**pAkt (%)**
16	105	**100**	2.9	58	26	0.08	2.4	**100**	7.6	74	7.4	0.57	13	**p-P70S6K (%)**
96	105	**100**	47	120	64	72	64	**100**	45	95	57	58	77	**pS6 (%)**

(B) Target Modulation in HuH-7 Cells

Veh	Veh	Vor	Pic	20f	20f	20e	20e	20o	20o	20q	20q	Sor	Sor	Sample
-	-	10	1	10	1	10	1	10	1	10	1	10	1	Conc. (μM)
-	+	+	+	+	+	+	+	+	+	+	+	+	+	VEGF

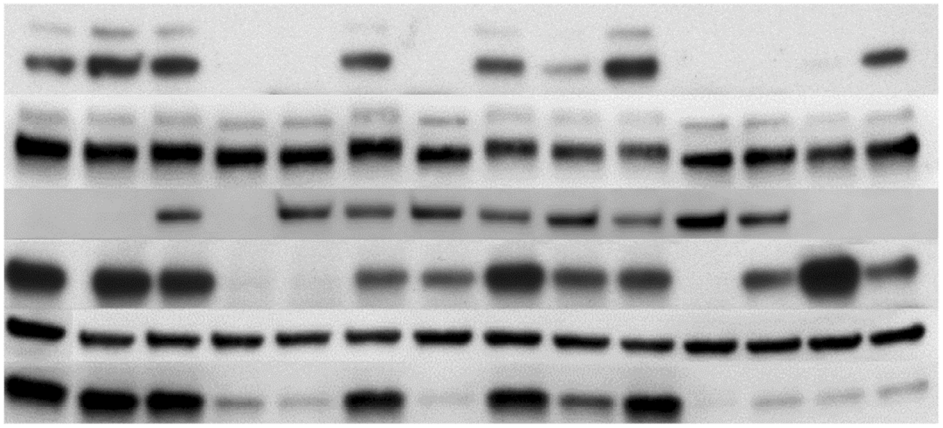

2.8	3.8	130	5.3	142	**100**	126	89	113	60	182	141	8.0	2.1	**Ac-α-Tub (%)**
50	**100**	65	3.0	7.1	34	27	71	28	44	1.3	1.2	252	42	**pAkt (%)**
45	**100**	94	0	0	54	0.29	43	11	111	1.5	1.7	11	197	**p-P70S6K (%)**
44	**100**	84	14	14	71	7.6	52	34	80	4.7	5.6	5.3	5.8	**pS6 (%)**

Figure 5. Modulation of HDACs and PI3K/Akt/mTOR pathway in liver cancer cells. (A). HepG2 cells were serum starved overnight (20 h), then treated with vehicle (0.1% DMSO) or compounds for 4 h, followed by stimulation with growth factors FGF2 (50 ng/mL), IGF-1 (100 ng/mL) and EGF (50 ng/mL) for 15 min, respectively. Veh: vehicle. (B) HuH-7 cells were treated with vehicle (0.1% DMSO) or compounds in serum free media for 4 h including last 12 min stimulated with VEGF (20 ng/mL). Vor: vorinostat; Pic: pictilisib; Sor: sorafenib.

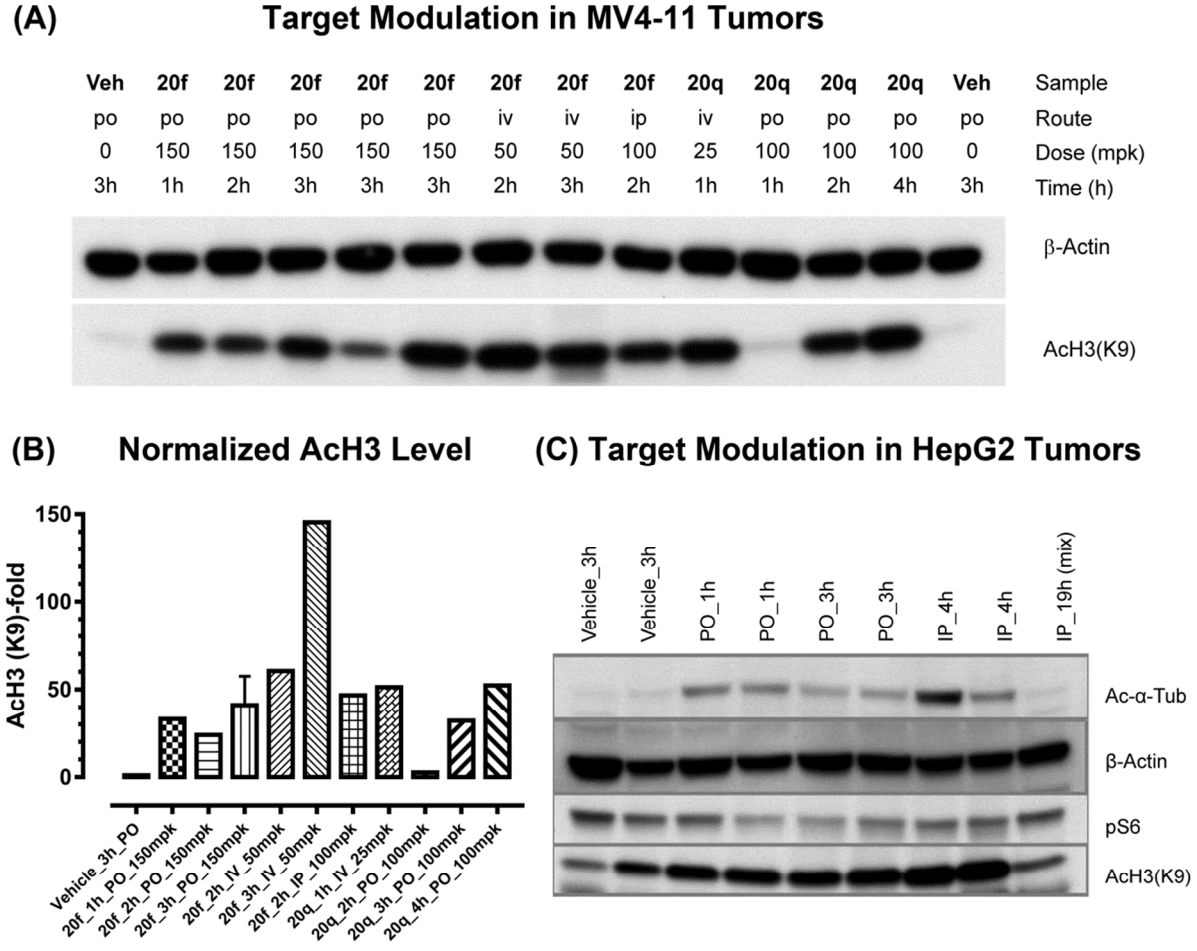

Figure 6. Modulation of HDACs in tumor-bearing mice models. (A) Hyperacetylation of H3 in MV4-11 tumors induced by **20f** and **20q**. Tumor bearing BALB/c nude mice were treated with vehicle [DMSO/PEG400/sterile water (10:40:50)] (3 h, po, 10 mL/kg), **20f** which was

administered in three routes (po, 150 mg/kg; iv, 50 mg/kg and ip, 100 mg/kg), and **20q** which was administered in two routes (po, 100 mg/kg and iv, 25 mg/kg). (B) Intensity of normalized AcH3 (Lys9) bands in Figure A. (C) Hyperacetylation of H3 and α-tubulin in HepG2 tumors induced by **20f**. Tumor bearing NCr nude mice were treated with vehicle (3 h, po, 10 mL/kg) and **20f** which was administered in two routes: po (150 mg/kg, 1 h and 3 h) and ip (75 mg/kg, 4 h and 19 h).

The effective concentration (EC_{50}) to modulation the targets in cancer cells were also determined by in-cell ELISA. For instance, after 3 h drug treatment of MCF7 cells, EC_{50} values for Ac-α-tubulin were 0.43, 0.19, 0.22, and >30 μM for vorinostat, **20f**, **20q** and pictilisib, respectively. In HepG2 cells, after 3 h of drug treatment and EGF stimulation, EC_{50} values for pAkt(S473) reduction were >30, 0.58, 0.13, and 0.17 μM for vorinostat, **20f**, **20q**, and pictilisib, respectively.

Modulation of Targets in Mice Bearing Tumors. MV4-11 tumor bearing mice were treated with **20f** via iv (50 mg/kg), ip (100 mg/kg) and po (150 mg/kg) routes, **20q** via both iv (25 mg/kg) and po (100 mg/kg) routes for pharmacodynamics (PD) assessment. All three routes of administration of **20f** resulted in hyperacetylation of H3 in MV4-11 tumors (Figure 6A). **20q** also induced hyperacetylation of H3 via both routes of administration. The western blot data of AcH3 were normalized and presented in Figure 6B, it was apparent the iv route was more efficient due to its bioavailability. **20f** was also evaluated via two route of administration in HepG2 xenograft model (Figure 6C), further confirmed the modulation of HDACs (i.e.,

hyperacetylation of H3 and α-tubulin, gain of signal), while modulation of Akt/mTOR was less significant (reduction of signal).

In Vitro ADME Profiling. In general, these compounds (Table 8) have reasonable lipophilicity, and were very stable in human liver microsomal stability assays. They didn't show significant inhibition of the hERG channel protein (IC_{50} > 100 μM), while **3** had an IC_{50} of 79.5 μM. In human liver microsomes (HLM) based CYP3A4 inhibition assay (IPA CYP3A4 substrate), compounds **20h**, **20f**, **20e** and sorafenib did not show significant inhibition on CPY3A4 (IC_{50} >10 μM). **20f** demonstrated low clearance in human liver microsomal stability assays (Table 8) as compared to its mouse and rat liver microsomal data. As CYP3A4 is responsible for metabolism of majority of the drugs, **20f** was tested with human recombinant CYP3A4 and found of low clearance (Table 9), while CYP3A4 substrates verapamil, midazolam and sorafenib showed higher clearance. Sorafenib and regorafenib are mainly metabolized by CYP3A4; hence it is less likely that **20f** would affect their metabolism in vivo when either of them combines with **20f** in a combination therapy.

Table 8. Microsomal Stability ($t_{½}$, min), Lipophilicity and hERG Inhibition

Compd	Microsomal Stability ($t_{½}$, min)			Lipophilicity		Safety (hERG)
	HLM[a]	MLM[a]	RLM[a]	LogP[b]	$LogD_{pH7.4}$[c]	IC_{50} (μM)[d]
20c	>60	>60	36	2.52	NT	NT
20e	>60	>60	37	1.80	1.71	>100
20f	>60	>60	55	2.34	2.07	>100
20h	>60	>60	35	0.75	NT	>100
20m	>60	8.7	25	1.83	NT	NT
20n	>60	33	50	3.30	NT	NT
20o	>60	>60	>60	1.47	2.14	>100
20q	>60	39	NT	1.63	1.97	>100
20t	>60	>60	>60	2.35	NT	NT
29	>60	23	20	2.64	NT	NT
DXM	>60	13	10	3.56	NT	NT
Verapamil	27	14	15	4.66	NT	NT
Vorinostat	NT	NT	NT	1.78	1.05	NT
3	NT	NT	NT	1.53	3.07	79.5

[a]See experimental section, microsomes protein 0.5 mg/mL. [b]LogP (Molecular Networks) Calculated using ChemBioOffice Ultra 13.0. [c]*n*-Octanol/water, pH 7.4. [d]Tested by Life Technologies using the Predictor® hERG Fluorescence Polarization assay. NT: not tested. DXM: dextromethorphan

Table 9. Metabolic Stability of 20f and Reference Compounds

	Clearance			
	Microsomes (μL/min/mg of protein) [a]			P450 (μL/min/pmol-P450) [b]
Compd	HLM	MLM	RLM	rCYP3A4
20f	10.4	26.8	25.5	0.19
Verapamil	73.0	99.1	93.9	2.36
DXM	20.2	111.8	140.8	NT
Midazolam	NT	NT	NT	3.73
Sorafenib	NT	NT	NT	4.38

[a]Test compounds (5 μM) were incubated with human liver microsomes (0.5 mg/mL) and NADPH (1.3 mM) at pH 7.4. [b]Test compounds (5 μM) were incubated with recombinant human CYP3A4 (25 nM) and NADPH (1.3 mM) at pH 7.4. Compound concentration was determined by LC–MS. NT: not tested. DXM: dextromethorphan.

Pharmacokinetics (PK) and Tissue Distribution. The lead compounds were scaled up and evaluated in a number of animals studies and the initial efforts were focused on **20f**. PKs (po, ip and iv) in a variety of formulations were investigated. **20f** is a hydroxamate and its PK profile was similar to that of hydroxamate-based oral HDAC inhibitors such as vorinostat and panobinostat: fast absorption and higher clearance in plasma (Table 10). In a quick 4 h PK study, the bioavailability of **20f** was 5.8% when dosed as a suspension at 50 mg/kg. When dosed as a clear formulation at 150 mg/kg, the 24 h bioavailability was 18%, and the terminal half-life was 4.4 h, which was similar to the intravenous terminal half-life of 4.6 h. The PK profile in mice was more or less similar to hydroxamates such as vorinostat, belinostat and panobinostat

which showed F% = 8.3%, 6.7%, and 4.6%, respectively. [46] Limited tissue distribution and PK/PD studies confirmed the favorable drug enrichment in tumors and target tissues (i.e., liver for HCC). For example, Hep3B tumor bearing mice were treated with **20f** (po, 100 mg/kg), AUCs (1 h to 24 h) of liver and Hep3B tumor were 21- and 5.4-fold as that of plasma, respectively (Figure 7). Drug in tumor tissue had a similar terminal half-life as that of plasma (6.5 h vs 6.0 h), but the drug in liver had a much longer terminal half-life of 11.1 h. The drug concentrations in the tumor were significantly higher than the enzymatic IC_{50} values (HDAC1, 1.1 nM; PI3Kα, 28 nM) as well as cellular IC_{50} values (Hep3B, 1.25 μM; HepG2, 0.59 μM) or colony formation IC_{50} values (Hep3B, 0.61 μM; HepG2, 0.10 μM). Thus drug concentration was reasonably high enough to inhibit the tumor growth even though the protein binding yet to be considered.

Table 10. PK Parameters of Compound 20f

	Routes of Administration		
Parameters	iv	po	po
Dose (mg/kg)	50	50	150
Dose (μmol/kg)	110	110	330
Formulation[a]	DPW	DMCTW	DSW
$AUC_{0-\infty}$ (μM•h)	16.68	0.97	9.06
T_{max} (h)		0.17	0.5
$T_{½}$ (h)	4.59	2.01	4.41
T_{last} (h)	24	4[b]	24
C_{max} (μM)		3.90	10.1
CL (L/h/kg)	6.60		
Vss (L/kg)	3.06		
F (%)		5.8	18.1

[a]Formulation: DPW = DMSO/PEG400/sterile water [10:40:50 (v/v)]; DMCTW = DMSO/MC-TW (0.5% Methyl Cellulose + 0.1% Tween 80 in water) [5:95 (v/v)]; DSW = DMSO/Solutol HS15/Sterile Water [7:18:45 (v/v)]. [b]Quick PK analysis, incomplete terminal elimination curve.

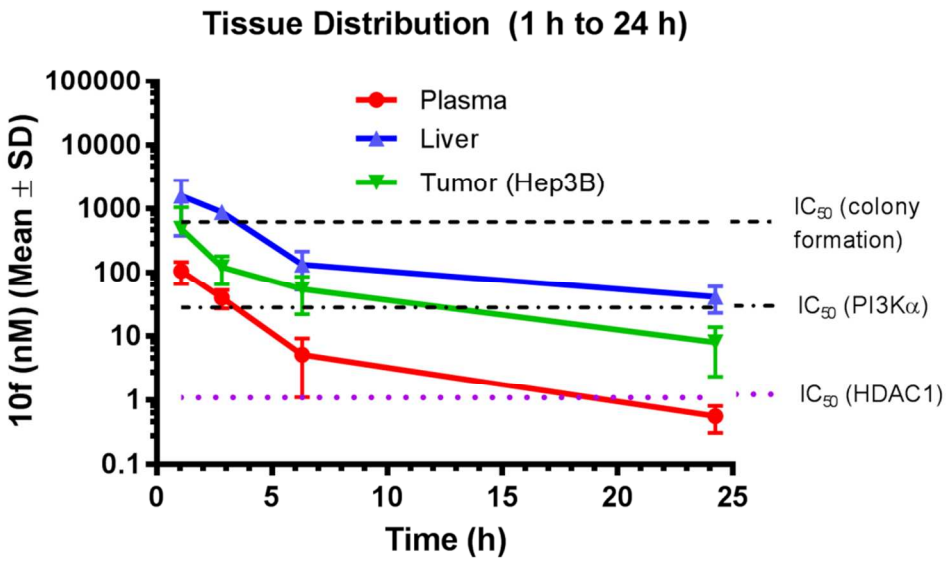

Figure 7. Tissue distribution of **20f** (po, 100mg/kg) in Hep3B tumor bearing NCr nude mice. AUCs (1 h to 24 h) of liver (▲) and Hep3B tumor (▼) were 21- and 5.4-fold as that of plasma (●), respectively. Drug in tumor tissue had a similar terminal half-life as plasma (6.5 h vs 6.0 h), but the drug in liver had a longer terminal half-life of 11.1 h.

Maximum Tolerable Dose (MTD). **20e**, **20f**, **20o** and **20q** were scaled up and evaluated their MTD in BALB/c mice. When **20f** formulated in DMSO/Solutol HS15/Water (DSW, v/v, 7:18:45), both dosage regimens 150 mg/kg QD×5 and 200 mg/kg QD×5 were found well-tolerated, but both dosage regimens 150 mg/kg BID and 100 mg/kg BID×5 were lethal, thus 200 mg/kg QD×5 was the MTD, and 150 mg/kg QD×5 per week was selected as the highest dose for long term of treatment. **20e** was dosed up to 150 mg/kg (salt form, freebase 130 mg/kg) in DSW formulation with pTSA, QD×5, and was well-tolerated, no significant body weight loss (−1.4% on day 5), MTD was not reached due to the limitation of compound supply. **20q** was troublesome to formulate due to its low solubility. In female NCr nude mice, 75 mg/kg QD×5

(5day-on-2day-off) was toxic, but at 50 mg/kg, QD×5 per week for 3 weeks, no loss of bodyweight was observed, hence the MTD was estimated at about 65 mg/kg for **20**q. MTD for **20o** was found at 150 mg/kg QD×5 or higher. The following efficacy studies were focused on **20f** and **20e** as both were easy to afford clear and stable formulations.

In Vivo Antitumor Efficacy Studies. In vivo oral efficacy of **20f** and **20e**, along with reference compound sorafenib and a combination for HDAC/PI3K dual inhibition (the combination of vorinostat with pictilisib), were evaluated in liver cancer models (e.g., HepG2, Hep3B, and HuH-7) (Table 11 and Figure 8).

Oral Efficacy in HepG2 NCr Mice Xenograft Model. Both **20f** and **20e** were tested in HepG2 models. In the first experiment (Table 11), **20f** (150 mg/kg, QD×5 per week) demonstrated significant oral efficacy in HepG2 xenograft model with tumor growth inhibition (TGI) values of 91% and 95% on day 14 and 18 (after last dose), respectively (Table 11). Reference sorafenib tosylate (98 mg/kg) was less effective with TGI values of 56% (day 14) and 72% (day 18), respectively. In another HepG2 xenograft experiment, **20e** was also demonstrated efficacy with TGI of 57% (day 14) after two cycles of treatment. The combination of HDAC inhibitor vorinostat (60 mg/kg) with PI3K inhibitor pictilisib (75 mg/kg) was used to mimic the dual inhibition of both HDAC and PI3K, with half MTD or highest reported dose for each reference inhibitor. MTD of vorinostat in clear DSW solution was 120 mg/kg as we measured in a previous experiment. The highest daily dose of pictilisib in xenograft models was 150 mg/kg. [30] For combination therapy, half MTD of vorinostat and half highest daily dosage of pictilisib were used, it is actually the same combination previously used in Daudi NHL xenograft mouse model. [36]

Oral Efficacy in Hep3B Xenograft Model. At a lower dosage, 100 mg/kg, **20f** was still effectively inhibited Hep3B tumors (Table 11), achieved TGI values of 82% and 86% on day 21 and day 23, respectively. While TGI values for sorafenib (60 mg/kg) were 71% and 73%, respectively. Bodyweight loss was observed for all groups, probably due to the DCW formulation (DMSO/ Cremophor EL /water = 1:3:6, v/v) used, dosage regimen of the first week (QD×7) applied, as well as the increased tumor burden.

Oral Efficacy in HuH-7 Models. HuH-7 tumor-bearing NCr nude mice were treated with either vehicle or **20f** (150 mg/kg) from Day 0 (QD×5 per week or per cycle). In HuH-7 models, **20f** was efficacious against established bigger tumors (day 0, 363 mm^3) with TGI value of 78% (day 12, $p = 0.0221$) (Table 11), sorafenib was dosed at 80 mg/kg with TGI value of 61% (day 12, $p = 0.1054$).

Oral Efficacy in CB17 Scid Mice HepG2 Xenograft Model. As **20f** showed excellent antitumor activity in HepG2 tumor bearing NCr nude mice, it was further evaluated for dose-response in female CB17 scid mice (Figure 8). When the HepG2 tumor size was about 240 mm^3 in average, tumor-bearing mice were randomized and dosed orally with vehicle, **20f** (150, 75 and 37.5 mg/kg) and sorafenib tosylate for four weeks (QD×5 per week) on day 0. **20f** demonstrated significant tumor inhibition in a dose-dependent manner (Figure 8A). After last dose of the fourth cycle, on day 26, TGI = 117%, 82%, 38% and 98% for **20f** (150, 75 and 37.5 mg/kg) and sorafenib tosylate, respectively. **20f** was well-tolerated at all dose levels (Figure 8B). Significant TGI with 5/5 regression in 150 mg/kg group (po, QD×5/week) were achieved. (Figure 8C and Figure 8D).

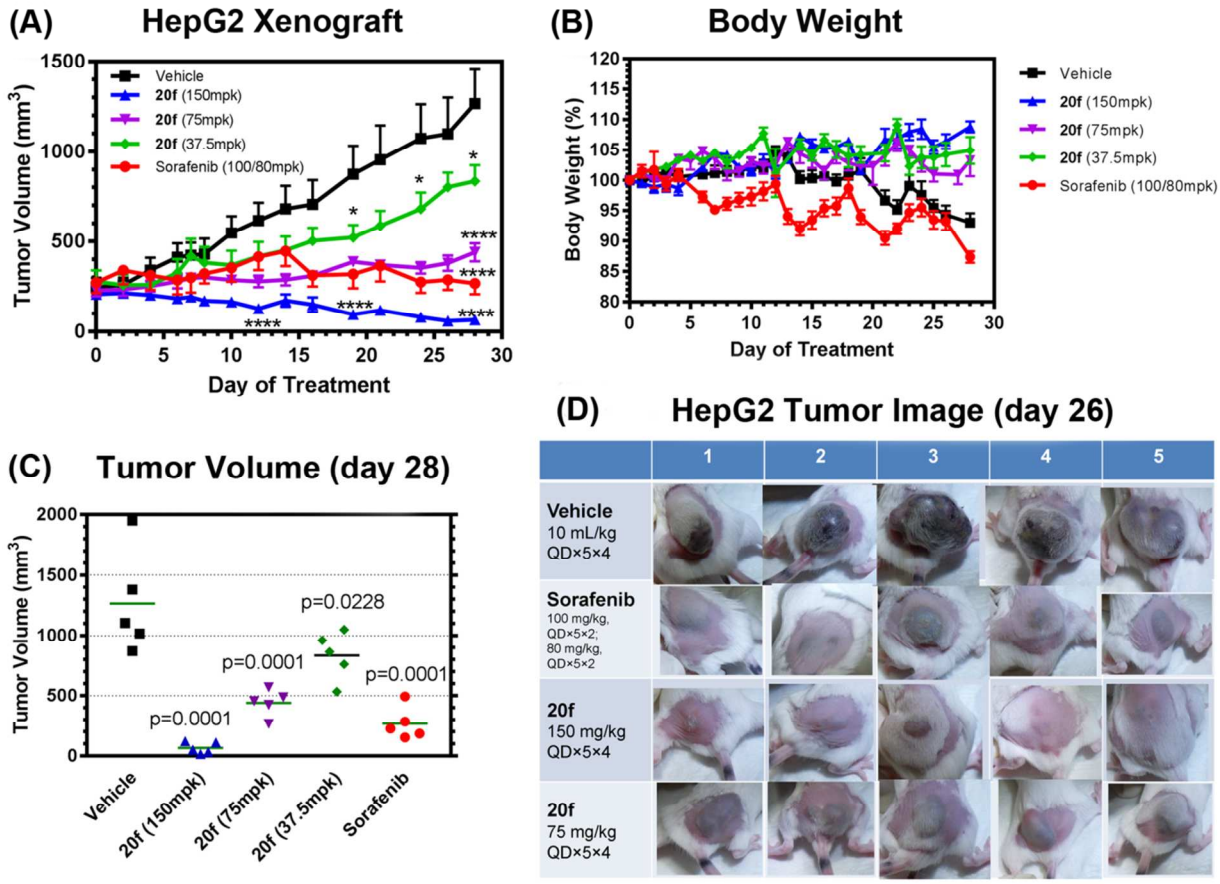

Figure 8. Dose-response of **20f** in HepG2 xenograft model. (A) HepG2 tumor-bearing CB17 scid mice were treated orally with vehicle (**20f**, 150 (▲), 75 (▼) and 37.5 (♦) mg/kg, and sorafenib tosylate (●, 100 mg/kg QD×5×2 then 80 mg/kg, QD×5×2) for 4 weeks (QD×5 per week) from day 0 with mean tumor volume about 240 mm^3. Tumor volume (*y* axis) is expressed as mean ± SEM. * $p < 0.05$, ** $p < 0.01$, *** $p < 0.001$ and **** $p \leqslant 0.0001$. (B) **20f** was well-tolerated at all dose levels, no significant body weight (BW) loss. Vehicle group has BW loss due to increasing tumor burden. Sorafenib tosylate (100 mg/kg) was not well-tolerated; its dose was reduced to 80 mg/kg in the third and fourth cycles. (C) Tumor volume at day 28 after 4 cycles of treatment. (D) Tumor image of mice on day 26, after last dose of the fourth cycle.

Table 11. Efficacy of Orally Administered 20f and 20e in Various Xenograft Models

Tumor model [a]	Compd [b]	Schedule (po) [c]	Dose (mg/kg) [d]	%TGI (day) [e]	Statistical Significance (day) [f]	Body weight change (%)(day) [g]	Survivors (day) [h]
HepG2	Vehicle	QD×5/wk ×3	---	---	---	+7.1 (14) +4.4 (18)	9/9 (18)
	20f	QD×5/wk ×3	150	91 (14) 95 (18)	* (14) ** (18)	+4.1 (14) +3.5 (18)	6/6 (32)
	Sorafenib	5-on-1-off ×3	98	56 (14) 72 (18)	ns (14) * (18)	−2.4 (14) −2.0 (18)	5/5 (26)
HepG2	Vehicle	QD×5/wk ×2	---	---	---	−0.8 (14)	5/5 (14)
	20e	QD×5/wk ×2	130	57 (14)	* (14)	−2.2 (5)	5/5 (14)
	Vorinostat + Pictilisib	QD×5/wk ×2	[60+75]	51 (14)	* (14)	−4.5 (12) −3.1 (14)	5/5 (12) 4/5 (14)
Hep3B	Vehicle	QD×7 + 2-off-5-on ×2	---	---	---	-8.9 (15)	6/6 (23)
	20f	QD×7 + 2-off-5-on ×2	100	82 (21) 86 (23)	** (21) ** (23)	−13.2 (18)	7/7 (23)
	Sorafenib	QD×7 + 2-off-5-on ×2	60	71 (21) 73 (23)	* (21) * (23)	−10.3 (16)	5/5 (23)
HuH-7	Vehicle		---	---	---	−2.1 (12)	10/10 (19)
	20f	QD×5/wk ×2	150	78 (12)	* (12)	−0.9 (12)	5/5 (22)

Tumor model [a]	Compd [b]	Schedule (po) [c]	Dose (mg/kg) [d]	%TGI (day) [e]	Statistical Significance (day) [f]	Body weight change (%)(day) [g]	Survivors (day) [h]
	Sorafenib	QD×5/wk ×2	80	61 (12)	ns (12)	−5.2 (9)	5/5 (23)

[a]Female NCr nude mice (CrTac:NCr-*Foxn1*^{nu}, 5–6 weeks of age, InVivos Pte Ltd, Singapore) were inoculated in the right flank with liver cancer cell lines HepG2 (6×10^6), HuH-7 (6×10^6), or Hep3B (3.6×10^6) in 50% Matrigel. [b]Compounds **20e**, **20f**, vorinostat and pictilisib were formulated in DMSO/Solutol HS15/sterile water (v/v, 7:18:45). Small crystals of p-Toluenesulfonic acid monohydrate (pTSA) were added to **20e** and pictilisib formulation to make clear solution (final pH 2–3). [c]Dose schedule: po, QD×5/wk = once daily for 5 days of treatment and 2 days without treatment (5-day-on-2-day-off) per week (wk); 5-on-1-off: QD×5 with 1 day holiday in 6-day cycle; 2-off-5-on: 2 days holiday, then QD×5. [d]Dose: vehicle dosed at 10 mL/kg. Vorinostat and pictilisib were dosed at 60 mg/kg and 75 mg/kg for combination, respectively. [e]The percent tumor growth inhibition (% TGI) = $(C_t - T_t)/(C_t - C_0) \times 100$. C_0 and C_t are the mean tumor volumes for control group (vehicle) on day 0 (first day of the treatment) and day t, respectively. T_t is the mean tumor volume for treatment group on day t. [f] Two-tailed unpaired t Test was used for comparing two groups, and one-way ANOVA followed by Dunnett's Multiple Comparison Test was used for comparing three and more groups to determine the statistical significance of tumor volume between a treatment group and the control (vehicle) group, ns = not significant, * $p < 0.05$, ** $p < 0.01$, *** $p < 0.001$ and **** $p \leqslant 0.0001$. [g]Percentage body weight (BW) change was calculated by normalizing BW over day 0. Lowest %BW during the treatment period was reported as well as %BW on days of TGI calculated. [h]Survivors: the number of animals still alive when the treatment cycle completed or experiment terminated

To facilitate the future preclinical evaluations, **20f** was tested in formulations without DMSO. **20f** can be formulated in Solutol HS15 solution without DMSO, but overnight solubilization is necessary. Solubility of **20f** in non-toxic (2-hydroxypropyl)-β-cyclodextrin based formulation was over 30 mg/mL and the oral bioavailability of **20f** in such formulation was confirmed. **10q** and **20o** are yet to be evaluated with similar or new formulations.

Advanced HCC is generally resistant to chemotherapy, with sorafenib being the only FDA-approved drug for the first-line treatment of advanced HCC.[47] However its benefit is modest. For

advanced HCC patients that developed drug resistance to sorafenib or are intolerant of sorafenib, there is currently no established systemic therapy. Targeting vascular endothelial growth factor (VEGFR) like how sorafenib does to inhibit tumor angiogenesis is important and also effective, but a number of kinase inhibitors in this category have failed clinical trials.[48] As it might be difficult to outperform sorafenib in anti-angiogenesis, it is thus necessary to consider other targets/pathways which are significantly different from anti-VEGF because sorafenib or other similar class of drugs can take care of it very well. Our approach is to design and develop a multi-target drug to take care of additional and important targets/networks which are complementary to sorafenib therapy. These purine-based HDAC/PI3K inhibitors such as **20f** and **20e** had demonstrated oral efficacy in liver cancer models. With **3** in ongoing clinical trials and new purine-based analogues of **3** being reported recently,[49] these dual or multi-functional HDAC inhibitors have yet to be validated in clinics for their safety and efficacy.

Conclusions

A series of fused-pyrimidine based hydroxamates were designed, synthesized, and evaluated. They inhibited HDAC enzymes, PI3K kinases, and the cell proliferation of a variety of human tumor cell lines. Most of the compounds demonstrated good drug-like properties (i.e., in vitro metabolic stability, solubility, and desirable lipophilicity). Selected compounds **20f** and **20q** also showed target modulation in both cancer cells and mice bearing tumors (i.e., hyperacetylation of histone 3 and α-tubulin and reduction of pAkt). **20f** also demonstrated excellent single agent oral anti-antitumor activity in HCC models and 4T1 mouse metastatic breast cancer models (Supporting Information, Table S4). These multi-target drug molecules may have the potential to be combined with current approved drugs such as sorafenib or regorafenib or other emerging

therapies. With regards to immunotherapy, if it is successful in the treatment of HCC (e.g., nivolumab treatment of HCC patients) [50] or other cancers in near future (e.g., pembrolizumab in combination with entinostat, an HDAC inhibitor, in lung cancer and melanoma),[51-54] it will pave the way for more combinations of immunotherapy with HDAC inhibitors or multifunctional HDAC inhibitors. The encouraging single agent oral efficacy data in HCC models, along with its favorable target profiles and tissue distribution warrant further development of **20f**, either as monotherapy or, preferably, in combination with traditional approved drugs or immunotherapy. Other potential indications are for the treatment of subgroups of leukemia (i.e., AML) and non-Hodgkin lymphomas (i.e., diffuse large B-cell lymphoma).

Experimental Section

Chemistry. Reagents were purchased from commercial suppliers, such as Sigma-Aldrich Pte Ltd (Singapore 117528, Singapore), Boron Molecular Inc. (Raleigh, NC 27616, USA), or Combi-Blocks, Inc. (San Diego, CA 92126, USA). CEM Discover Microwave Reactor was used for some reactions. Analytical thin-layer chromatography (TLC) was performed on glass-backed silica gel 60 F 254 plates (E Merck (0.25 mm)) and eluted with the appropriate solvent ratios (v/v) and visualized by UV absorption. The reactions were assayed by TLC and/or LC–MS and terminated as judged by the consumption of starting material or the formation of desire product. Flash column chromatography was conducted using silica gel 60 (Merck KGaA, 0.040–0.063 mm, 230–400 mesh ASTM). Reverse-phase preparative high performance liquid chromatography (RPHPLC) was conducted on a Gilson HPLC system (331/332 pumps, GX-271 liquid handler, 172 diode array doctor (DAD), Trilution LC software) using a Phenomenex column (Luna, 5 μm, C18 100A, 150 mm x 21.2 mm) with adjustable solvent gradients, usually 5–95% of acetonitrile in water + 0.05% TFA in 15 or 20 min of gradient at flow rate of 20

mL/min, and was used for routine purification. The preliminary purity and identity of all compounds after purification were assessed by LC–MS analyses on a Waters Micromass ZQ mass spectrometer in electrospray ionization (ESI) positive mode after separation on a Waters 2795 separations module. The HPLC separations were performed on a Phenomenex column (Luna, 5 μm, C18 100A, 50 mm × 2.00 mm) with a flow rate of 0.8 mL/min and a 4-min gradient of X–95% (X = 5, 30 or 50) of acetonitrile in water + 0.05% TFA, using a Waters 2996 photodiode array detector (Method A) or with a flow of 0.6 mL/min and a 6-min gradient of X–95% (X = 5, 30 or 50) of methanol in water + 0.1% formic acid (Method B). Purity and identity were assessed on the integrated UV chromatograms (220–400 nm) and the mass spectra. The final purity was determined using a Shimadzu LC-20AD UFLC system on a Phenomenex column (Luna, 5 μm, C18 100A, 50 mm × 2.00 mm) with a flow rate of 0.8 mL/min and a 6-min gradient of X–95% (X = 5, 30 or 50) of acetonitrile in water + 0.05% TFA (Method C). A longer column (Phenomenex® Gemini 5 micron C18, 110A, 4.6×150 mm) together with a flow rate of 1.0 ~1.2 mL/min and a 15-min gradient of 5–95% acetonitrile in water + 0.05% TFA was also used for purity check (Method D). Purity was >95% for all target compounds.

All NMR experiments were performed on a Bruker AVANCE-400 digital NMR spectrometer. NMR spectra are reported in ppm with reference to an internal tetramethylsilane standard (0.00 ppm for ^{1}H and ^{13}C) or solvent peak(s) of $CDCl_3$ (7.26 and 77.1 ppm) or CD_3OD (3.31 and 49.0 ppm), or DMSO-d_6 (2.50 and 39.5 ppm). Other NMR solvents were used as needed. Elemental analyses of CHN were performed on a Perkin-Elmer 2400 CHN/CHNS Elemental Analyzers. HRMS results were obtained from a Bruker micrOTOF-Q II (ESI, positive mode) with direct injection of purified compounds.

Compounds **17a**–**d** were synthesized by procedures used for **17d**.

4-(6-(2-Aminopyrimidin-5-yl)-2-morpholino-9*H*-purin-9-yl)-*N*-hydroxybutanamide (**17a**). Obtained as powder (30 mg, 34%). LC–MS *m/z*: $[M + H]^+$ 400.1. HPLC purity (254 nm): 99.9%. ^{1}H NMR (DMSO-d_6, 400 MHz): δ 10.34 (s, 1H), 9.55 (s, 2H), 8.25 (s, 1H), 7.50 (s, 2H), 4.14 (t, J = 6.4 Hz, 2H), 3.82–3.77 (m, 4H), 3.75–3.70 (m, 4H), 2.11–2.01 (m, 2H), 2.01–1.93 (m, 2H).

5-(6-(2-Aminopyrimidin-5-yl)-2-morpholino-9*H*-purin-9-yl)-*N*-hydroxypentanamide (**17b**). Obtained as powder (22 mg, 38%). LC–MS *m/z*: $[M + H]^+$ 414.1. HPLC purity (254 nm): 98.6%. ^{1}H NMR (DMSO-d_6, 400 MHz): δ 10.34 (s, 1H), 9.54 (s, 2H), 8.25 (s, 1H), 7.45 (s, 2H), 4.14 (t, J = 6.4 Hz, 2H), 3.82–3.77 (m, 4H), 3.75–3.70 (m, 4H), 1.99 (t, J = 7.2 Hz, 2H), 1.86–1.76 (m, 2H), 1.52–1.41 (m, 2H).

6-(6-(2-Aminopyrimidin-5-yl)-2-morpholino-9*H*-purin-9-yl)-*N*-hydroxyhexanamide (**17c**). Obtained as powder (41 mg, 38%). LC–MS *m/z*: $[M + H]^+$ 428.1. HPLC purity (254 nm): 95.8%. ^{1}H NMR (DMSO-d_6, 400 MHz): δ 10.32 (s, 1H), 9.54 (s, 2H), 8.24 (s, 1H), 7.42 (s, 2H), 4.12 (t, J = 6.8 Hz, 2H), 3.82–3.76 (m, 4H), 3.75–3.69 (m, 4H), 1.95 (t, J = 7.6 Hz, 2H), 1.88–1.77 (m, 2H), 1.61–1.49 (m, 2H), 1.29–1.17 (m, 2H).

7-(6-(2-Aminopyrimidin-5-yl)-2-morpholino-9*H*-purin-9-yl)-*N*-hydroxyheptanamide (Scheme 1, 17d)

Step 1. N-Alkylation. To a pre-stirred solution of 2,6-dichloro-9*H*-purine **11a** (376 mg, 2.0 mmol), ethyl 7-bromoheptanoate (521 mg, 2.2 mmol) in DMF (15 mL), was added anhydrous potassium carbonate (552 mg, 4.0 mmol) and NaI (64 mg, 0.4 mmol). The resulting mixture was stirred at 40 °C for 12 h and the reaction was completed as indicated by LC–MS. After workup, the crude was purified by flash chromatography (silica, ethyl acetate/hexanes from 1:3 to 1:2) to afford ethyl 7-(2,6-dichloro-9H-purin-9-yl)heptanoate (**13d)** (480 mg, 69%). LC–MS *m/z*: $[M + H]^+$ 345.1. ^{1}HNMR ($CDCl_3$, 400 MHz): δ 8.26 (s, 1H), 4.34 (t, J = 7.2 Hz, 2H), 4.12 (q, J = 7.1

Hz, 2H), 2.30 (t, J = 7.3 Hz, 2H), 1.99 (quint, J = 6.6 Hz, 2H), 1.63 (quint, J = 7.1 Hz, 2H), 1.48–1.35 (m, 4H), 1.26 (t, J = 7.1 Hz, 3H). ^{13}C NMR ($CDCl_3$, 100 MHz): δ 173.3, 153.2, 152.6, 151.3, 146.1 (CH), 130.6, 60.1, 44.5, 33.8, 29.4, 28.3, 26.1, 24.5, 14.2.

Step 2. Suzuki coupling. To a pre-stirred solution of **13d** (344 mg, 1.0 mmol), 5-(4,4,5,5-tetramethyl-1,3,2-dioxaboro+lan-2-yl)pyrimidin-2-amine **14a** (240 mg, 1.1 mmol) in dioxane (15 mL), was added a solution of K_2CO_3 (345 mg, 2.5 mmol) in DI water (2.0 mL). The mixture was degassed for 30 min then was added Pd(dppf)Cl_2·CH_2Cl_2 (41 mg, 0.05 equiv). The resulting mixture was heated at 82 °C for 6 h. LC–MS showed the reaction completed. After workup, the crude was purified by flash chromatography (silica, 33% to 50% to 100% of ethyl acetate in hexanes) to afford ethyl 7-(6-(2-aminopyrimidin-5-yl)-2-chloro-9*H*-purin-9-yl)heptanoate (**15d**) (150 mg, 37%). LC–MS *m/z*: $[M + H]^+$ 404.1.

Step 3. Displacement with morpholine. To a pre-stirred solution of **15d** (150 mg, 0.37 mmol) in DMF (5 mL), was added morpholine (0.70 mL, 3.0 mmol). The resulting mixture was heated at 80 °C for 12 h. After workup, ethyl 7-(6-(2-aminopyrimidin-5-yl)-2-morpholino-9*H*-purin-9-yl)heptanoate (**16d**) (120 mg, 72%) was obtained by recrystallization of the crude in 10% MeOH in DCM. LC–MS *m/z*: $[M + H]^+$ 455.1.

Step 4. Hydroxamic acid formation. To a pre-stirred solution of **16d** (70 mg, 0.155 mmol), hydroxylamine hydrochloride (108 mg, 1.55mmol) in dry MeOH (1.5 mL), pre-cooled down over dry ice, was added slowly with sodium methoxide solution (25 wt.% in methanol, 4.37 M) (901 μL, 3.88 mmol). The resulting mixture was stirred at −20 °C for 1 h before it was warmed up to rt. LC–MS showed the reaction completed after 3 h. After workup, the crude was purified by RPHPLC to afford **17d** (15 mg, 21%). LC–MS *m/z*: $[M + H]^+$ 442.1. HPLC purity (254 nm): 96.6%. ^{1}H NMR (DMSO-d_6, 400 MHz): δ 10.34 (s, 1H), 9.54 (s, 2H), 8.25 (s, 1H), 7.45 (s,

2H), 4.12 (t, 2H, *J* = 6.8 Hz), 3.82–3.77 (m, 4H), 3.76–3.71 (m, 4H), 1.93 (t, *J* = 7.2 Hz, 2H), 1.87–1.77 (m, 2H), 1.52–1.43 (m, 2H), 1.36–1.18 (m, 4H). HRMS (ESI) *m/z*: $[M + H]^+$ calcd for $C_{20}H_{27}N_9O_3$, 442.2310; found, 442.2308.

Compounds **20a–s** were synthesized by procedures used for **20f**.

7-(2,6-Dimorpholino-9*H*-purin-9-yl)-*N*-hydroxyheptanamide (**20a**). LC–MS *m/z*: $[M + H]^+$ 434.2. HPLC purity (254 nm): 96.5 %. ^{1}H NMR (DMSO-d_6, 400 MHz): δ 10.31 (s, 1H), 7.87 (s, 1H), 4.27–4.05 (m, 4H), 4.00 (t, *J* = 6.9 Hz, 2H), 3.68 (t, *J* = 4.7 Hz, 4H), 3.66–3.58 (m, 8H), 1.91 (t, *J* = 7.3 Hz, 2H), 1.74 (quint, *J* = 6.9 Hz, 2H), 1.45 (quint, *J* = 7.3 Hz, 2H), 1.33–1.14 (m, 4H).

***N*-Hydroxy-6-(2-(6-methoxypyridin-3-yl)-6-morpholino-9*H*-purin-9-yl)hexanamide** (**20b**). LC–MS *m/z*: $[M + H]^+$ 442.2. HPLC purity (254 nm): 95.7%. ^{1}H NMR (DMSO-d_6, 400 MHz): δ 10.33 (s, 1H), 9.15 (d, *J* = 2.0 Hz, 1H), 8.58 (dd, *J* = 8.7 and 2.3 Hz, 1H), 8.22 (s, 1H), 6.92 (d, *J* = 8.7 Hz, 1H), 4.40–4.25 (m, 4H), 4.22 (t, *J* = 6.9 Hz, 2H), 3.93 (s, 3H), 3.77 (t-like, *J* = 4.6 Hz, 4H), 1.94 (t, *J* = 6.8 Hz, 2H), 1.87 (quint, *J* = 7.3 Hz, 2H), 1.57 (quint, *J* = 7.5 Hz, 2H), 1.25 (quint, *J* = 6.9 Hz, 2H). HRMS (ESI) *m/z*: $[M + H]^+$ calcd for $C_{21}H_{28}N_7O_4$, 442.2197; found, 442.2204.

***N*-Hydroxy-7-(2-(6-methoxypyridin-3-yl)-6-morpholino-9*H*-purin-9-yl)heptanamide** (**20c**). LC–MS *m/z*: $[M + H]^+$ 456.1. HPLC purity (254 nm): 98.8 %. ^{1}H NMR (DMSO-d_6, 400 MHz): δ 10.34 (s, 1H), 9.15 (d, *J* = 2.0 Hz, 1H), 8.58 (dd, *J* = 8.7 and 2.4 Hz, 1H), 8.22 (s, 1H), 6.92 (d, *J* = 8.6 Hz, 1H), 4.38–4.25 (br s, 4H), 4.22 (t, *J* = 7.0 Hz, 2H), 3.93 (s, 3H), 3.77 (t, *J* = 4.6 Hz, 4H), 1.93 (t, *J* = 7.2 Hz, 2H), 1.86 (quint, *J* = 6.9 Hz, 2H), 1.48 (quint, *J* = 7.1 Hz, 2H), 1.36–1.21 (m, 4H). HRMS (ESI) *m/z*: $[M + H]^+$ calcd for $C_{22}H_{29}N_7O_4$, 456.2354; found, 456.2369.

6-(2-(6-Aminopyridin-3-yl)-6-morpholino-9*H*-purin-9-yl)-*N*-hydroxyhexanamide (**20d**). LC–MS *m/z*: $[M + H]^+$ 427.2. HPLC purity (254 nm): 96.5%. ^{1}H NMR (DMSO-d_6, 400 MHz): δ 10.33 (s, 1H), 8.79–8.73 (m or overlapped dd, 1H), 8.75 (s, 1H), 8.43 (br s, 2H), 8.24 (s, 1H), 7.09 (d-like, *J* = 10.1 Hz, 1H), 4.40–4.23 (m, 4H), 4.20 (t, *J* = 6.9 Hz, 2H), 3.76 (t, *J* = 4.6 Hz, 4H), 1.93 (t, *J* = 7.3 Hz, 2H), 1.84 (quint, *J* = 7.3 Hz, 2H), 1.55 (quint, *J* = 7.5 Hz, 2H), 1.22 (quint, *J* = 7.3 Hz, 2H).

7-(2-(6-Aminopyridin-3-yl)-6-morpholino-9*H*-purin-9-yl)-*N*-hydroxyheptanamide (**20e**). Recrystallization of the freebase in MeOH with excess of formic acid afforded **20e** as formic acid "salt" (containing 1.0 ± 0.3 equivalent of formic acid as estimated by ^{1}H NMR). LC–MS *m/z*: $[M + H]^+$ 441.2. HPLC purity (254 nm): 97.3 %. ^{1}H NMR (DMSO-d_6, 400 MHz): formic acid salt. δ 10.32 (s, 1H), 8.93 (d, *J* = 1.9 Hz, 1H), 8.30 (dd, *J* = 8.7 and 2.2 Hz, 1H), 8.15 (s, 1H), 8.13 (s, 0.7H, formic acid), 6.52 (d, *J* = 8.7 Hz, 1H), 6.32 (br s, 2H), 4.38–4.22 (br s, 4H), 4.18 (t, *J* = 6.8 Hz, 2H), 3.75 (t, *J* = 4.3 Hz, 4H), 1.93 (t, *J* = 7.2 Hz, 2H), 1.84 (quint, *J* = 6.7 Hz, 2H), 1.48 (quint, *J* = 7.0 Hz, 2H), 1.38–1.22 (m, 4H). ^{13}C NMR (DMSO-d_6, 100 MHz): formic acid salt δ 169.0, 163.0, 160.5, 156.3, 152.9, 151.7, 148.3, 139.9, 136.4, 122.3, 117.6, 107.2, 66.2, 45.2 (br), 42.6, 32.1, 29.1, 27.9, 25.7, 24.9. HRMS (ESI) *m/z*: $[M + H]^+$ calcd for $C_{21}H_{29}N_8O_3$, 441.2357; found, 441.2374. Anal. ($C_{21}H_{28}N_8O_3 \cdot 0.7H_2O \cdot HCO_2H$) C, N. H: calcd, 6.34; found, 6.84.

***N*-Hydroxy-7-(2-(3-(hydroxymethyl)phenyl)-6-morpholino-9*H*-purin-9-yl)heptanamide (Scheme 2, 20f)**

Step 1. Displacement with morpholine. To a pre-stirred solution of **13d** (172 mg, 0.5 mmol) in DCM (5 mL), was added morpholine (218 mg, 2.5 mmol). The resulting mixture was stirred at 40 °C for 3 h. After simple workup, the crude product was purified by flash chromatography

(silica, ethyl acetate/hexanes from 1:3 to 1:2) to afford ethyl 7-(2-chloro-6-morpholino-9*H*-purin-9-yl)heptanoate (**18d**) (170 mg, 87%). LC–MS *m/z*: $[M + H]^+$ 397.2. ^{1}HNMR ($CDCl_3$, 400 MHz): δ 7.70 (s, 1H), 4.56–4.11 (m, 6H), 4.12 (q, *J* = 7.2 Hz, 2H), 3.82 (t, *J* = 4.6 Hz, 4H), 2.27 (t, *J* = 7.2 Hz, 2H), 1.92–1.79 (m, 2H), 1.60 (quint, *J* = 7.0 Hz, 2H), 1.42–1.27 (m, 4H), 1.24 (t, *J* = 7.0 Hz, 3H). ^{13}C NMR ($CDCl_3$, 100 MHz): δ 173.6, 153.94, 153.93, 152.2, 118.6, 66.9, 60.3, 45.7(br), 43.8, 34.1, 29.8, 28.5, 26.3, 24.7, 14.3.

Step 2. Suzuki coupling. To a pre-stirred solution of **18d** (100 mg, 0.254 mmol), (3-(hydroxymethyl)phenyl)boronic acid (**14f**, 76 mg, 0.5 mmol) in dioxane (5.0 mL), was added with potassium carbonate (86 mg, 0.62 mmol) and $Pd(dppf)Cl_2 \cdot CH_2Cl_2$ (10 mg). The resulting mixture was stirred at 150 °C for 1 h under the microwave irradiation. LC–MS showed the reaction completed after 1 h. After removing the solvent, the crude was suspended in DCM and purified by flash chromatography (silica, 1% to 2% MeOH in DCM) to afford ethyl 7-(2-(3-(hydroxymethyl)phenyl)-6-morpholino-9*H*-purin-9-yl)heptanoate (**19f**) (30 mg, 25%). LC–MS m/z: $[M + H]^+$ 468.3. ^{1}HNMR (DMSO-d_6, 400 MHz): δ 8.34 (s, 1H), 8.27(dt-like, *J* = 7.2 Hz, 1H), 8.22 (s, 1H), 7.42 (t, *J* = 7.5 Hz, 1H), 7.39 (dt-like, *J* = 7.5 Hz, 1H), 5.27 (t, *J* = 5.0 Hz, 1H), 4.58 (d, *J* = 4.4 Hz, 2H), 4.38–4.25 (br s, 4H), 4.23 (t, *J* = 6.8 Hz, 2H), 4.01 (q, *J* = 7.2 Hz, 2H), 3.77 (t, *J* = 4.8 Hz, 4H), 2.24 (t, *J* = 7.2 Hz, 2H), 1.86 (quint, *J* = 7.2 Hz, 2H), 1.49 (quint, *J* = 7.4 Hz, 2H), 1.38–1.20 (m, 4H), 1.14 (t, *J* = 7.0 Hz, 3H). ^{13}C NMR (DMSO-d_6, 100 MHz): δ 173.3, 157.3, 153.5, 152.3, 142.9, 141.1, 138.6, 128.4, 128.3, 126.7, 126.2, 118.7, 66.7, 63.5, 60.1, 45.6, 43.2, 33.8, 29.5, 28.2, 26.1, 24.7, 14.5.

Step 3. Hydroxamic acid formation and scale-up. To a pre-stirred solution of **19f** (30 mg, 0.064 mmol), hydroxylamine hydrochloride (67 mg, 0.96 mmol) in dry MeOH (1.0 mL), pre-cooled down over dry ice, was added slowly with sodium methoxide solution (25 wt.% in methanol,

0.37 mL, 1.62 mmol). The resulting mixture was stirred at −20 °C for 1 h before it was warmed up to rt. LC–MS showed the reaction completed after 2 h. After simple workup, the mixture was purified by RPHPLC to afford **20f** as white solid (8 mg, 22% as calcd as TFA salt), HPLC purity (254 nm): 97.4%. Scale-up of freebase: the **20f** TFA salt made from **19f** (500 mg) was dissolved in acetonitrile and water, and then basified using saturated aqueous $NaHCO_3$ to pH around 8. After removal of acetonitrile under reduced pressure, the aqueous solution was extracted with ethyl acetate (×3). The combined organic layers was dried and evaporated, and the resulting product was further purified by recrystallization in MeOH to afford **20f** as freebase (381 mg, 78%): LC–MS *m/z*: $[M + H]^+$ 455.1. HPLC purity (254 nm): 98.4%. ^{1}H NMR (DMSO-d_6, 400 MHz): δ 10.32 (s, 1H), 8.65 (s, 1H), 8.35 (s or t-like, 1H), 8.27 (dt-like, *J* = 7.3 Hz, 1H), 8.22 (s, 1H), 7.43 (t, *J* = 7.5 Hz, 1H), 7.39 (dt-like, *J* = 7.5 Hz, 1H), 5.29 (t-like, 1H), 4.58 (d, *J* = 3.8 Hz, 2H), 4.40–4.26 (m, 4H), 4.23 (t, *J* = 6.9 Hz, 2H), 3.77 (t, *J* = 4.6 Hz, 4H), 1.92 (t, *J* = 7.3 Hz, 2H), 1.86 (quint, *J* = 6.8 Hz, 2H), 1.47 (quint, *J* = 7.1 Hz, 2H), 1.36–1.20 (m, 4H) ; ^{13}C NMR (DMSO-d_6, 100 MHz): δ 169.0, 156.9, 153.0, 151.8, 142.5, 140.6, 138.2, 128.0, 127.9, 126.2, 125.8, 118.2, 66.3, 63.0, 45.1 (br), 42.8, 32.1, 29.1, 28.0, 25.7, 25.0. HRMS (ESI) *m/z*: $[M + H]^+$ calcd for $C_{23}H_{30}N_6O_4$, 455.2402; found, 455.2405. Anal. ($C_{23}H_{30}N_6O_4 \cdot 0.25H_2O$) C, H, N.

***N*-Hydroxy-7-(2-(4-hydroxymethyl)phenyl)-6-morpholino-9*H*-purin-9-yl)heptanamide** (**20g**). LC–MS *m/z*: $[M + H]^+$ 455.2. HPLC purity (254 nm): 97.0 %. ^{1}H NMR (DMSO-d_6, 400 MHz): δ 10.32 (s, 1H), 8.35 (d, *J* = 8.2 Hz, 2H), 8.21 (s, 1H), 7.41 (d, *J* = 8.3 Hz, 2H), 4.56 (s, 2H), 4.40–4.25 (br s, 4H), 4.22 (t, *J* = 7.0 Hz, 2H), 3.77 (t, *J* = 4.6 Hz, 4H), 1.92 (t, *J* = 6.6 Hz, 2H), 1.85 (quint, *J* = 6.7 Hz, 2H), 1.46 (quint, *J* = 6.9 Hz, 2H), 1.36–1.20 (m, 4H).

7-(2-(2-Aminopyrimidin-5-yl)-6-morpholino-9*H*-purin-9-yl)-*N*-hydroxyheptanamide (**20h**). LC–MS *m/z*: 442.1 $[M + H]^+$. HPLC purity (254 nm): 97.8 %. ^{1}H NMR (DMSO-d_6, 400

MHz): δ 10.31 (s, 1H), 9.10 (s, 2H), 8.66 (br s, 1H), 8.16 (s, 1H), 7.04 (s, 2H), 4.40–4.22 (m, 4H), 4.18 (t, J = 6.8 Hz, 2H), 3.75 (t-like, J = 4.0 Hz, 4H), 1.92 (t, J = 7.2 Hz, 2H), 1.83 (quint, J = 6.6 Hz, 2H), 1.47 (quint, J = 6.9 Hz, 2H), 1.36–1.19 (m, 4H). HRMS (ESI) *m/z*: $[M + H]^+$ calcd for $C_{20}H_{27}N_9O_3$, 442.2310; found, 442.2326.

***N*-Hydroxy-7-(2-(4-(methylsulfonamido)phenyl)-6-morpholino-9*H*-purin-9-yl)heptanamide** (**20i**). LC–MS *m/z*: $[M + H]^+$ 518.1. HPLC purity (254 nm): 96.7 %. ^{1}H NMR (DMSO-d_6, 400 MHz): δ 10.33 (s, 1H), 9.96 (s, 1H), 8.34 (d, 2H, J = 8.8 Hz), 8.21 (s, 1H), 7.30 (d, J = 8.8 Hz, 2H), 4.42–4.25 (m, 4H), 4.22 (t, J = 7.0 Hz, 2H), 3.76 (t, J = 4.7 Hz, 4H), 3.05 (s, 3H), 1.92 (t, J = 7.3 Hz, 2H), 1.85 (quint, J = 6.9 Hz, 2H), 1.47 (quint, J = 7.1 Hz, 2H), 1.35–1.20 (m, 4H).

7-(2-(3-Acetamidophenyl)-6-morpholino-9*H*-purin-9-yl)-*N*-hydroxyheptanamide (**20j**). LC–MS *m/z*: $[M + H]^+$ 482.2. HPLC purity (254 nm): 98.8 %. ^{1}H NMR (DMSO-d_6, 400 MHz): δ 10.34 (s, 1H), 10.07 (s, 1H), 8.46 (s, 1H), 8.23 (s, 1H), 8.06 (d, J = 7.8 Hz, 1H), 7.82 (d, J = 7.9 Hz, 1H), 7.38 (t, J = 7.9 Hz, 1H), 4.80–4.25 (m, 4H), 4.22 (t, J = 6.9 Hz, 2H), 3.77 (t-like, J = 4.6 Hz, 4H), 2.08 (s, 3H), 1.92 (t, J = 7.3 Hz, 2H), 1.86 (quint, J = 6.8 Hz, 2H), 1.47 (quint, J = 7.1 Hz, 2H), 1.36–1.20 (m, 4H).

3-(9-(7-(Hydroxyamino)-7-oxoheptyl)-6-morpholino-9*H*-purin-2-yl)benzamide (**20k**). LC–MS *m/z*: $[M + H]^+$ 468.2. HPLC purity (254 nm): 99.2 %. ^{1}H NMR (DMSO-d_6, 400 MHz): δ 10.32 (s, 1H), 8.83 (t, J = 1.5 Hz, 1H), 8.53 (dt, J = 8.0 and 1.3 Hz, 1H), 8.25 (s, 1H), 8.11 (s, 1H), 7.93 (dt, J = 7.8 and 1.4 Hz, 1H), 7.55 (t, J = 7.7 Hz, 1H), 7.45 (s, 1H), 4.45–4.28 (m, 4H), 4.25 (t, J = 7.0 Hz, 2H), 3.78 (t, J = 4.6 Hz, 4H), 1.92 (t, J = 7.3 Hz, 2H), 1.87 (quint, J = 6.8 Hz, 2H), 1.47 (quint, J = 7.0 Hz, 2H), 1.35–1.20 (m, 4H).

4-(9-(7-(Hydroxyamino)-7-oxoheptyl)-6-morpholino-9*H*-purin-2-yl)benzamide (**20l**). LC–MS *m/z*: $[M + H]^+$ 468.2. HPLC purity (254 nm): 99.3 %. ^{1}H NMR (DMSO-d_6, 400 MHz): δ 10.33 (s, 1H), 8.43 (d, *J* = 8.4 Hz, 2H), 8.25 (s, 1H), 8.04 (s, 1H), 7.96 (d, *J* = 8.4 Hz, 2H), 7.45 (s, 1H), 4.40–4.26 (m, 4H), 4.24 (t, *J* = 7.0 Hz, 2H), 3.77 (t-like, *J* = 4.6 Hz, 4H), 1.92 (t, *J* = 7.3 Hz, 2H), 1.86 (quint, *J* = 6.8 Hz, 2H), 1.47 (quint, *J* = 7.0 Hz, 2H), 1.35–1.20 (m, 4H).

***N*-Hydroxy-7-(6-morpholino-2-(1*H*-pyrazol-4-yl)-9*H*-purin-9-yl)heptanamide** (**20m**). LC–MS *m/z*: $[M + H]^+$ 415.2. HPLC purity (254 nm): 97.3 %. ^{1}H NMR (DMSO-d_6, 400 MHz): δ 10.32 (s, 1H), 8.17 (s, 2H), 8.13 (s, 1H), 4.37–4.19 (m, 4H), 4.16 (t, *J* = 7.0 Hz, 2H), 3.74 (t-like, *J* = 4.8 Hz, 4H), 1.92 (t, *J* = 7.1 Hz, 2H), 1.82 (quint, *J* = 6.9 Hz, 2H), 1.47 (quint, *J* = 7.2 Hz, 2H), 1.35–1.18 (m, 4H). HRMS (ESI) m/z $[M + H]^+$ calcd for $C_{19}H_{26}N_8O_3$, 415.2201; found, 415.2214.

7-(2-(1*H*-Indazol-6-yl)-6-morpholino-9*H*-purin-9-yl)-*N*-hydroxyheptanamide (**20n**). LC–MS *m/z*: $[M + H]^+$ 465.2. HPLC purity (254 nm): 98.0 %. ^{1}H NMR (DMSO-d_6, 400 MHz): δ 10.36 (s, 1H), 8.58 (s, 1H), 8.24 (s, 1H), 8.22 (dd-like, *J* = 8.8 Hz, 1H), 8.11 (s, 1H), 7.82 (d, *J* = 8.8 Hz, 1H), 4.45–4.28 (m, 4H), 4.25 (t, *J* = 6.9 Hz, 2H), 3.79 (t, *J* = 4.6 Hz, 4H), 1.94 (t, *J* = 7.3 Hz, 2H), 1.86 (quint, *J* = 6.8 Hz, 2H), 1.49 (quint, *J* = 7.0 Hz, 2H), 1.40–1.22 (m, 4H).

***N*-Hydroxy-7-(2-(2-methoxypyrimidin-5-yl)-6-morpholino-9*H*-purin-9-yl)heptanamide** (**20o**). LC–MS *m/z*: $[M + H]^+$ 457.2. HPLC purity (254 nm): 97.5%. ^{1}H NMR (DMSO-d_6, 400 MHz): δ 10.32 (s, 1H), 9.40 (s, 2H), 8.65 (s, 1H), 8.25 (s, 1H), 4.47–4.25 (m, 4H), 4.22 (t, *J* = 6.9 Hz, 2H), 3.99 (s, 3H), 3.76 (t, *J* = 4.5 Hz, 4H), 1.92 (t, *J* = 7.3 Hz, 2H), 1.85 (quint, *J* = 6.7 Hz, 2H), 1.47 (quint, *J* = 7.0 Hz, 2H), 1.35–1.20 (m, 4H). ^{13}C NMR (DMSO-d_6, 100 MHz): δ 168.4, 165.0, 158.2, 152.7, 152.4, 150.8, 140.1, 125.2, 117.8, 65.6, 54.3, 45.1 (br), 42.3, 31.5,

28.5, 27.4, 25.1, 24.4. HRMS (ESI) *m/z*: $[M + H]^+$ calcd for $C_{21}H_{29}N_8O_4$, 457.2306; found, 457.2327.

7-(2-(4-Fluoro-3-hydroxyphenyl)-6-morpholino-9*H*-purin-9-yl)-*N*-hydroxyheptanamide (**20p**). LC–MS *m/z*: $[M + H]^+$ 459.1. HPLC purity (254 nm): 99.5 %. ^{1}H NMR (DMSO-d_6, 400 MHz): δ 10.35 (s, 1H), 9.98 (br s, 1H), 8.20 (s, 1H), 8.04 (dd, *J* = 9.0 and 2.0 Hz, 1H), 7.83 (ddd, *J* = 8.5, 4.5 and 2.1 Hz, 1H), 7.20 (dd, *J* = 11.1 and 8.6 Hz, 1H), 4.40–4.23 (m, 4H), 4.20 (t, *J* = 7.0 Hz, 2H), 3.76 (t, *J* = 4.7 Hz, 4H), 1.93 (t, *J* = 7.3 Hz, 2H), 1.85 (quint, *J* = 6.9 Hz, 2H), 1.47 (quint, *J* = 7.1 Hz, 2H), 1.35–1.20 (m, 4H).

7-(2-(2-Aminopyrimidin-5-yl)-4-morpholino-7*H*-pyrrolo[2,3-d]pyrimidin-7-yl)-*N*-hydroxyheptanamide (**20q**). LC–MS *m/z*: $[M + H]^+$ 441.2. HPLC purity (254 nm): 99.8 %. ^{1}HNMR (DMSO-d_6, 400 MHz): δ 10.31 (s, 1H), 9.12 (s, 2H), 8.66 (s, 1H), 7.27 (d, *J* = 3.6 Hz, 1H), 6.97 (s, 2H), 6.65 (d, *J* = 3.6 Hz, 1H), 4.20 (t, *J* = 6.8 Hz, 2H), 3.92 (t, *J* = 4.6 Hz, 4H), 3.76 (t, *J* = 4.6 Hz, 4H), 1.92 (t, *J* = 7.3 Hz, 2H), 1.78 (quint, *J* = 7.0 Hz, 2H), 1.46 (quint, *J* = 7.3 Hz, 2H), 1.37–1.17 (m, 4H). ^{13}C NMR (DMSO-d_6, 100 MHz): δ 169.0, 163.8, 157.4, 156.5, 153.1, 151.5, 124.6, 120.9, 100.9, 100.6, 66.1, 45.4, 43.5, 32.2, 29.5, 28.0, 25.7, 25.0. HRMS (ESI) *m/z*: $[M + H]^+$ calcd for $C_{21}H_{29}N_8O_3$, 441.2357; found, 441.2373. Anal. ($C_{21}H_{28}N_8O_3$) H, N. C: calcd, 57.26; found, 57.72.

***N*-Hydroxy-7-(2-(3-hydroxyphenyl)-4-morpholino-7*H*-pyrrolo[2,3-d]pyrimidin-7-yl)heptanamide** (**20r**). LC–MS *m/z*: $[M + H]^+$ 440.1. HPLC purity (254 nm): 100.0 %. ^{1}HNMR (DMSO-d_6, 400 MHz): δ 10.34 (br s, 1H), 7.86–7.82 (m, 2H), 7.34 (d, *J* = 3.6 Hz, 1H), 7.25 (t, *J* = 8.0 Hz, 1H), 6.81 (ddd, *J* = 8.0, 2.4 and 1.1 Hz, 1H), 6.68 (d, *J* = 3.6 Hz, 1H), 4.23 (t, *J* = 6.9 Hz, 2H), 3.94 (t, *J* = 4.7 Hz, 4H), 3.78 (t, *J* = 4.7 Hz, 4H), 1.91 (t, *J* = 7.3 Hz, 2H), 1.80 (quint, *J*

= 7.0 Hz, 2H), 1.46 (quint, *J* = 7.3 Hz, 2H), 1.35–1.16 (m, 4H). HRMS (ESI) *m/z*: $[M + H]^+$ calcd for $C_{23}H_{30}N_5O_4$, 440.2292; found, 440.2306.

6-(2-(4-Fluoro-3-hydroxyphenyl)-6-morpholino-9*H*-purin-9-yl)-*N*-hydroxyhexanamide (**20s**). LC–MS *m/z*: $[M + H]^+$ 445.2. HPLC purity (254 nm): 98.0%. ^{1}H NMR (DMSO-d_6, 400 MHz): δ 10.34 (br s, 1H), 8.21 (s, 1H), 8.03 (dd, *J* = 8.9 and 1.9 Hz, 1H), 7.83 (ddd, *J* = 8.4, 4.5 and 2.1Hz, 1H), 7.19 (dd, *J* = 10.9 and 8.6 Hz, 1H,), 4.40–4.24 (m, 4H), 4.21 (t, *J* = 6.9 Hz, 2H), 3.76 (t, *J* = 4.5 Hz, 4H), 1.93 (t, *J* = 7.2 Hz, 2H), 1.85 (quint, *J* = 7.3 Hz, 2H), 1.55 (quint, *J* = 7.5 Hz, 2H), 1.23 (quint, *J* = 6.5 Hz, 2H).

***N*-Hydroxy-7-(2-(3-(2-hydroxyethoxy)phenyl)-6-morpholino-9*H*-purin-9-yl)heptanamide** (**20t**). Ethyl 7-(2-(3-hydroxyphenyl)-6-morpholino-9*H*-purin-9-yl)heptanoate (**19t**) was prepared by procedures used for **19f** but starting from **18d** and (3-hydroxyphenyl)boronic acid (**14n**). **19t** (152.5 mg, 0.34 mmol), 2-bromoethanol (127.5 mg, 1.02 mmol), K_2CO_3 (235 mg, 1.7 mmol) in DMF (3.5 mL) was heated at 90 °C to drive the reaction to completion. The mixture was diluted with water and extracted with ethyl acetate. After workup, the crude was purified by flash chromatography (silica, 30% to 50% ethyl acetate in hexanes) to afford ethyl 7-(2-(3-(2-hydroxyethoxy)phenyl)-6-morpholino-9*H*-purin-9-yl)heptanoate (**19t2**) (36.2 mg, 21%) which was converted to hydroxamic acid **20t** by procedures used for **20f**. LC–MS *m/z*: $[M + H]^+$ 485.2. HPLC purity (254 nm): 99.1 %. ^{1}H NMR (DMSO-d_6, 400 MHz): δ 10.31 (s, 1H), 8.22 (s, 1H), 7.96 (d, *J* = 8.0 Hz, 1H), 7.92–7.89 (m, 1H), 7.35 (t, *J* = 7.8 Hz, 1H), 7.02 (dd, *J* = 7.8 and 2.2 Hz, 1H), 4.45–4.25 (m, 4H), 4.22 (t, overlapped, 2H), 4.10–4.00 (m, 2H), 3.85–3.70 (m, 6H), 1.92–1.88 (t, 2H), 1.88–1.83 (m, 2H), 1.50–1.40 (m, 2H), 1.35–1.20 (m, 4H).

7-(2-(4-Fluoro-3-(2-hydroxyethoxy)phenyl)-6-morpholino-9*H*-purin-9-yl)-*N*-hydroxyheptanamide (**20u**). It was synthesized similarly to **20t**. LC–MS *m/z*: $[M + H]^+$ 503.1.

HPLC purity (254 nm): 97.3 %. ^{1}H NMR (DMSO-d_6, 400 MHz): δ 10.32 (s, 1H), 8.23 (s, 1H), 8.12 (dd, J = 8.6 and 1.8 Hz, 1H), 7.98 (ddd, J = 8.4, 4.6 and 1.9 Hz, 1H), 7.30 (dd, J = 11.1 and 8.6 Hz, 1H), 4.40–4.25 (m, 4H), 4.22 (t, J = 6.9 Hz, 2H), 4.16 (t, J = 4.8 Hz, 2H), 3.79 (t, J = 4.9 Hz, 2H), 3.76 (t, J = 4.6 Hz, 4H), 1.92 (t, J = 7.3 Hz, 2H), 1.86 (quint, J = 6.8 Hz, 2H), 1.47 (quint, J = 7.0 Hz, 2H), 1.36–1.20 (m, 4H). HRMS (ESI) *m/z*: [M + H]+ calcd for $C_{24}H_{32}FN_6O_5$, 503.2413; found, 503.2432.

***N*-Hydroxy-7-(2-(3-(hydroxymethyl)-4-methoxyphenyl)-6-morpholino-9*H*-purin-9-yl)heptanamide** (**20v**). Ethyl 7-(2-(3-formyl-4-methoxyphenyl)-6-morpholino-9*H*-purin-9-yl)heptanoate (**19v**) was prepared by procedures used for **19f** but starting from **18d** and (3-formyl-4-methoxyphenyl)boronic acid (**14o**). **19v** (80 mg, 0.16 mmol) was reduced with $NaBH_4$ (60 mg, 1.6 mmol) in methanol and the crude was purified by flash chromatography (silica, 1% MeOH in DCM) to afford ethyl 7-(2-(3-(hydroxymethyl)-4-methoxyphenyl)-6-morpholino-9*H*-purin-9-yl)heptanoate (**19w**) (80 mg, >95%). **19w** was converted to hydroxamic acid **20v** by procedures used for **20f**. LC–MS *m/z*: $[M + H]^+$ 485.2. HPLC purity (254 nm): 97.9%. ^{1}H NMR (DMSO-d_6, 400 MHz): δ 10.32 (s, 1H), 8.43 (d, J = 2.2 Hz, 1H), 8.27 (dd, J = 8.6 and 2.2 Hz, 1H), 8.18 (s, 1H), 7.03 (d, J = 8.7 Hz, 1H), 4.54 (s, 2H), 4.35–4.25 (m, 4H), 4.21 (t, J = 6.9 Hz, 2H), 3.83 (s, 3H), 3.77 (t, J = 4.6 Hz, 4H), 1.92 (t, J = 7.2 Hz, 2H), 1.86 (quint, J = 6.9 Hz, 2H), 1.47 (quint, J = 7.2 Hz, 2H), 1.35–1.21 (m, 4H). HRMS (ESI) *m/z*: $[M + H]^+$ calcd for $C_{24}H_{33}N_6O_5$, 485.2507; found, 485.2506

7-(2-(2-Aminopyrimidin-5-yl)-6-(4-(hydroxymethyl)piperidin-1-yl)-9*H*-purin-9-yl)-*N*-hydroxyheptanamide (**23a**). LC–MS *m/z*: $[M + H]^+$ 470.1. HPLC purity (254 nm): 97.2%.^{1}H NMR (DMSO-d_6, 400 MHz): δ 10.34 (br s, 1H), 9.15 (s, 2H), 8.15 (s, 1H), 7.54 (br s, 2H), 4.18

(t, *J* = 6.9 Hz, 2H), 3.28 (d, *J* = 5.9 Hz, 2H), 3.08 (br s, 2H), 1.92 (t, *J* = 7.3 Hz, 2H), 1.88–1.68 (m, 5H), 1.47 (quint, *J* = 7.1 Hz, 2H), 1.35–1.10 (m, 6H).

7-(2-(2-Aminopyrimidin-5-yl)-6-(4-hydroxypiperidin-1-yl)-9*H*-purin-9-yl)-*N*-hydroxyheptanamide (**23b**). LC–MS *m/z*: ([M + H]$^+$ 456.1. HPLC purity (254 nm): 99.9%. ^{1}H NMR (DMSO-d_6, 400 MHz): δ 10.33 (br s, 1H), 9.12 (s, 2H), 8.14 (s, 1H), 7.25 (br s, 2H), 4.87 (m, 1H), 4.17 (t, *J* = 6.9 Hz, 2H), 3.84–3.75 (m, 2H), 3.74–3.57 (m, 2H), 1.96–1.76 (m, 6H), 1.52–1.36 (m, 4H), 1.35–1.19 (m, 4H).

(*E*)-*N*-Hydroxy-3-(4-(((2-(2-(6-methoxypyridin-3-yl)-6-morpholino-9*H*-purin-9-yl)ethyl)amino)methyl)phenyl)acrylamide (Scheme 4, 29)

Step 1. Displacement with morpholine. Morpholine (1.39 mL, 15.87 mmol) was added to a solution of **11a** (1.00 g, 5.29 mmol) in THF (26 mL). The resulting mixture was stirred at rt for 16 h. White precipitate was observed immediately upon addition of morpholine. The white precipitate was filtered off and washed with water (×2) and methanol (×2) to afford 4-(2-chloro-9*H*-purin-6-yl)morpholine (**24**) (1.13 g, 90%). LC–MS *m/z*: [M + H]$^+$ 240.1.

Step 2. N-Alkylation. To a solution of **24** (1.18 g, 4.94 mmol) in acetonitrile/DMSO (19:1) was added 2-iodoacetonitrile (0.71 mL, 9.87 mmol) and K_2CO_3 (1.36 g, 9.87 mmol). The resulting mixture was heated at 60 °C for 3 h. Then the solvents were removed in vacuo and water was added. The aqueous layer was extracted with DCM (×2) and the combined organic layers was washed with brine, dried over $MgSO_4$ and evaporated in vacuo. The resulting crude oil was purified by flash chromatography (silica, 50% ethyl acetate in hexanes) to afford 2-(2-chloro-6-morpholino-9*H*-purin-9-yl)acetonitrile (**25**) (1.31 g, 95%) as pale brown solid. LC–MS *m/z*: [M + H]$^+$ 279.1.

Step 3. Reduction. To a stirred solution of **25** (1.23 g, 4.42 mmol) and $NiCl_2 \cdot 6H_2O$ (105 mg, 0.44 mmol) in MeOH/THF (2:1) was added sodium borohydride (1.17 g, 30.97 mmol) in portions. The resulting mixture was allowed to stir at rt for 1 h. Then the solvents were removed in vacuo and a saturated solution of sodium bicarbonate was added. The aqueous layer was extracted with DCM (×2) and the combined organic layers was washed with brine, dried over $MgSO_4$ and evaporated in vacuo. The crude was purified by flash chromatography (silica, 10% methanol in DCM) to afford 2-(2-chloro-6-morpholino-9*H*-purin-9-yl)ethanamine (**26**) (577 mg, 46%) as colorless oil. LC–MS *m/z*: $[M + H]^+$ 283.1.

Step 4. Reductive amination. To a stirred solution of **26** (576 mg, 2.04 mmol) in DCE (10 mL) was added (*E*)-methyl 3-(4-formylphenyl)acrylate (466 mg, 2.45 mmol), acetic acid (0.12 mL, 2.04 mmol) and sodium triacetoxyborohydride (649 mg, 3.06 mmol) sequentially. The resulting mixture was stirred at rt for 5 h. A saturated solution of sodium bicarbonate was added to quench the reaction and the aqueous layer was extracted with DCM (×2). The combined organic layers was washed with brine, dried over $MgSO_4$ and evaporated in vacuo. The crude was purified by flash chromatography (silica, 4% methanol in DCM) to afford (*E*)-methyl 3-(4-(((2-(2-chloro-6-morpholino-9*H*-purin-9-yl)ethyl)amino)methyl)phenyl)acrylate (**27**) (414 mg, 44%) as off-white solid. LC–MS *m/z*: $[M + H]^+$ 457.2.

Steps 5 and 6. By following procedures of Suzuki coupling and hydroxamic acid formation used for **20f**, the title compound (**29**) was obtained as TFA salt. LC–MS *m/z*: $[M + H]^+$ 531.3. HPLC purity (254 nm): 96.2%. ^{1}HNMR (DMSO-d_6, 400 MHz): 400 MHz)br s, 1H), 9.14 (d, *J* = 2.2 Hz, 1H), 9.06 (br s, 2H), 8.52 (dd, *J* = 8.8 and 2.3 Hz, 1H), 8.19 (s, 1H), 7.55 (d, *J* = 8.1 Hz, 2H), 7.45 (d, *J* = 7.8 Hz, 2H), 7.42 (d, overlapped, 1H), 6.87 (d, *J* = 8.7 Hz, 1H), 6.46 (d, *J* = 15.9 Hz, 1H), 4.59 (t, *J* = 5.5 Hz, 2H), 4.44–4.19 (m, 6H), 4.10–3.66 (m, 2H), 3.91 (s, 3H), 3.76

(t-like, J = 4.5 Hz, 4H), 3.65–3.52 (m, 2H). HRMS (ESI) *m/z*: $[M + H]^+$ calcd for $C_{27}H_{31}N_8O_4$, 531.2463; found, 531.2473.

(*E*)-3-(4-(((2-(2-(2-Aminopyrimidin-5-yl)-6-morpholino-9*H*-purin-9-yl)ethyl)amino)methyl)phenyl)-*N*-hydroxyacrylamide (**31**). **31** was prepared by procedures used for **29**. LC–MS *m/z*: $[M + H]^+$ 517.2. HPLC purity (254 nm): 97.8%. ^{1}HNMR (DMSO-d_6, 400 MHz): δ 10.80 (br s, 1H), 9.14 (s, 2H), 9.00 (br s, 2H), 8.15 (s, 1H), 7.57 (d, J = 7.9 Hz, 2H), 7.45 (d, J = 7.9 Hz, 2H), 7.43 (d, overlapped, 1H), 7.15 (br s, 2H), 6.47 (d, J = 15.9 Hz, 1H), 4.57 (t, J = 5.3 Hz, 2H), 4.40–4.20 (m, 4H), 3.90–3.50 (m, 8H). HRMS (ESI) *m/z*: $[M + H]^+$ calcd for $C_{29}H_{29}N_{10}O_3$, 517.2419; found, 517.2421.

***N*-Hydroxy-4-(((2-(2-(6-methoxypyridin-3-yl)-6-morpholino-9*H*-purin-9-yl)ethyl)amino)methyl)benzamide** (**34**). **34** was analogously prepared by procedures used for **29**. LC–MS *m/z*: $[M + H]^+$ 505.1. HPLC purity (254 nm): 97.3%. ^{1}HNMR (DMSO-d_6, 400 MHz): δ 11.28 (br s, 1H), 9.17 (d, J = 1.9 Hz, 1H), 9.08 (br s, 2H), 8.55 (dd, J = 8.7 and 2.4 Hz, 1H), 8.19 (s, 1H), 7.75 (d, J = 8.2 Hz, 2H), 7.50 (d, J = 8.3 Hz, 2H), 6.89 (dd, J = 8.7 and 0.5 Hz, 1H), 4.60 (t, J = 5.8 Hz, 2H), 4.40–3.95 (m, 6H), 3.92 (s, 3H), 3.75 (t, J = 4.6 Hz, 4H), 3.59 (t-like, 2H).

HDAC Enzyme Assay. HeLa nuclear extracts were prepared in-house and were used as the source of HDACs in routine HDAC inhibition assays. The recombinant HDAC enzymes, HDAC1 (Cat #5005), HDAC3/NcoR2 (Cat #50003), HDAC4 (Cat #50004), HDAC6 (Cat #50006), HDAC8 (Cat #50008) were purchased from BPS Bioscience Inc., United States. The assay was performed in 96-well format (black NBS half-area 96-well plate, Corning #3993) using a fluorescent-based HDAC activity assay. Substrates Boc-Lys(Ac)-AMC (Cat # I-1875) for HeLa nuclear extracts, HDACs 1, 2, 3, 6, and 10, Boc-Lys(Tfa)-AMC (Cat # I-1985) for

HDACs 4, 5, 7, 8, 9 and 11 were purchased from Bachem AG, Switzerland. The reaction mixture (50 μL/well) was composed of assay buffer (25 mM Tris, pH 8.0, 137 mM NaCl, 2.7 mM KCl, 1 mM $MgCl_2$, and 0.1 mg/mL BSA), test compounds, an appropriate concentration of enzyme, and 50 μM of substrate, and it was incubated at rt for 2 h. The reaction was stopped by addition of developer [50 μL/well, containing trypsin (Cat #T4799, Sigma-Aldrich), 2 mg/mL, 50 mM Tris pH 8.0, and LAQ824 (CAS 404951-53-7), 4.5 μM] and incubated at 37 ºC for 30 min. The fluorescence was detected at the excitation wavelength of 360 nm and emission wavelength of 460 nm using a BioTek Synergy H4 Hybrid Multi-Mode Microplate Reader and raw data were processed using BioTek's Gen5 (v2.03.01) software. Vorinostat (SAHA) was used as positive control.

Kinase Enzyme Assay. Lipid kinases PI3Kα: Cat # PV4788 from Invitrogen, or Cat # 40620 from BPS Bioscience Inc., United States; p110α(H1047R)/p85α (Cat #40641) from BPS, p110α(E545K)/p85α (Cat #P27-15H) from SignalChem; PI3Kβ: Cat # P28-10H (SignalChem), Cat # 40622 (BPS), PI3Kδ: Cat # P30-10H (SignalChem) were used in the ADP-Glo™ Kinase Assay (Promega). Serially diluted compounds solutions (5 μL/well, 3-fold, 8-concentration) were added to a white NBS half-area 96-well plate (Corning #3992). Lipid PIP2:PS (1:3) mixture (0.167 mg/mL: 0.5 mg/mL) in Lipid Dilution Buffer (25 mM HEPES, pH7.5, 0.5 mM EGTA) was diluted (1:1) with Reaction Buffer (3.33×) (159 mM HEPES, pH7.5, 87 mM NaCl, 9.5 mM $MgCl_2$, 0.08 mg/mL BSA) to make a 1.67× working solution, PI3K enzyme was diluted with the 1.67× working solution and 15 μL/well was used for reaction. ATP (125 μM, 5 μL/well) in DI water was added to initiate the reaction. After reaction at rt for 1 h, the reaction was stopped by addition of ADP-Glo solution (25 μL/well) and incubated at rt for 40 min, then kinase detection solution (50 μL/well) was added and incubated for 40 min, the luminescence

was read on a Biotek Synergy H4 Hybrid Multi-Mode Microplate Reader and raw data were processed using BioTek's Gen5 (v2.03.01) software. Pictilisib and wortmannin were used as positive controls. IC_{50} is defined as the concentration of compound required for 50% inhibition of enzyme activity.

Cell Culture and Anti-Proliferative Assays (Cellular IC_{50}). All cell lines were purchased directly from ATCC except HuH-7 which were obtained from Dr. Manikanden Lakshmanan (IMCB). Cells were cultivated at 37 °C, 5% CO_2 in recommended media containing 10% FBS. Antibiotics (100 U/mL of penicillin and 100 µg/mL of streptomycin) were added to the media used for compound dilution and cells in 96-well assay plates. For a typical screening experiment, cells (100 µL/well) were inoculated into 96-well microtiter plates at plating densities ranging from 2,000 to 30,000 cells/well depending on the doubling time of individual cell lines and assay linearity. After cell inoculation, the microtiter plates were incubated overnight (up to 24 h) prior to addition of compounds for adherent cells. Suspension cells were treated with test compounds immediately after cell inoculation. Test compounds were serially diluted (3-fold, 8-concentration) using the same media and added to the plates (15 to 25 µL/well). After 72 h of cultivation, the plates were assayed for cell cytotoxicity/viability by using the following two methods: Sulforhodamine B (SRB) method [55, 56] and CellTiter-Glo® Luminescent Cell Viability Assay. [57] The raw data were processed using BioTek's Software Gen5 (v2.03.01) to generate inhibitory IC_{50} values. Vorinostat was used as positive control.

Cell Line Authentication and Mycoplasma Detection. Cells were routinely monitored with MycoAlert™ PLUS Mycoplasma Detection Kit (Lonza Walkersville, Inc.) to make sure they were mycoplasma free. Genomic DNA was isolated according to manufacturer's protocol by using PureLink® Genomic DNA Mini Kit (Catalog Number K1820-01, Invitrogen, Carlsbad,

CA92008, USA). About 1×10^5 cells were used for DNA isolation. Cell line authentication was done at Genetica DNA Laboratories (1440 York Court, Burlington, NC 27215 USA) as well as in-house at The DNA Sequencing Facility (DSF, IMCB) by using Promega PowerPlex® 16 HS System and Promega GenePrint® 10 System, respectively. Cell line authentication data were verified and confirmed against ATCC database as well as published STR data. [58, 59] Mycoplasma detection was done at Genetica DNA Laboratories by using e-Myco™ plus Mycoplasma PCR Detection Kit (iNtRON Biotechnology).

Caspase Activity Assays. Cells were cultivated and treated with test compounds in 96-well plates as described in the above Cell Culture and Anti-Proliferative Assays section. Caspase assay buffer [100 mM HEPES (pH7.5), 200 mM NaCl，4 mM EDTA, 0.1% CHAPS, and freshly added 5 mM DTT and 50 μM of caspase substrate Z-DEVD-R110 or (Z-Asp-Glu-Val-Asp)$_2$-Rhodamine 110 (Cat #M-2615, Bachem, Switzerland)] was added to cells (100 μL/well) and the plates were incubated at rt and monitored for the caspase activity on a BioTek Synergy H4 reader (excitation: 496/9 nm, emission: 521/9 nm). Positive control was staurosporine.

Cell Viability/Cytotoxicity Assay. The content of dead cells and viable cells were measured using CytoTox-Glo™ Cytotoxicity Assay kit (Promega) per manufacture's protocol. Briefly, CytoTox-Glo™ Cytotoxicity Assay Reagent (48 μL/well) was added to the cells in 96-well plate and the luminescent signals were recorded using a BioTek Synergy H4 reader, then Lysis Reagent (48 μL/well) was added and the luminescent signals derived from both dead and viable cells were recorded. Viability was calculated by subtracting the luminescent signal resulting from experimental cell death from total luminescent values. Staurosporine was used as positive control.

Target Modulation of HDACs and PI3K/AKT/mTOR Pathway in Cancer Cells and Tumors. Western Blot Analysis. Cells were cultivated and treated with test compounds as described in the above Cell Culture and Anti-Proliferative Assays section. Cells were washed with cold DPBS twice and cooled on ice and treated with lysis buffer [50 mM Tris (pH7.4), 2.5 mM β-glycerophosphate, 150 mM NaCl, 1% NP-40, 0.5% sodium deoxycholate, 0.1% SDS, 2 mM sodium orthovanadate，10 mM sodium fluoride，1 mM EDTA and freshly added protease inhibitor PMSF (0.1 mM) and protease inhibitor cocktail (Cat # 03969, Nacalai Tesque, Inc. or Cat. # 539134, Calbiochem)]. Lysates were cleared at 20,000×*g* for 20×2 min, and protein concentrations were determined using BCA Protein Assay Kit (Cat # 71285-3, Novagen, USA). Proteins in cell lysates were resolved by SDS-PAGE and transferred to PVDF and probed with appropriate primary and secondary antibodies. Histone H3 (acetyl K9) (Cat # 9649), Histone H3 (Cat #9715), Acetyl-α-Tubulin (Lys40) (Cat #5335), α-Tubulin (Cat #2125), pAkt (Ser473) (Cat #4060), anti-Akt(pan) (Cat # 4685), pS6 ribosomal protein (Ser240/244) (Cat # 5364), S6 ribosomal protein (Cat # 2217), Phospho-4E-BP1 (Thr37/46) (Cat #2855), P70S6 Kinase (Cat #2708), Phospho-P70 S6 Kinase (Thr389) (Cat #9234), and HRP-linked anti-rabbit IgG (Cat #7074) antibodies were purchased from Cell Signaling Technology, Inc., USA. Anti-β-actin (Cat #ab8227) was from Abcam, and anti-GAPDH-HRP (Cat # sc-25778-HRP) was from Santa Cruz Biotechnology, Inc. The protein bands were detected using Pierce ECL Western Blotting Substrate (Cat #3229) and captured using FUJI Super RX-N films which were subsequently scanned and analyzed using ImageJ (1.47V) software. Or the gel signals were captured and processed using ChemiDoc™ Touch Imaging System with Image Lab™ Touch Software (Version 5.2.1 build 11, Nov 14, 2014, Bio-Rad Laboratories).

In Vitro ADME and Drug-like Properties. Lipophilicity (logD at pH 7.4), solubility, and microsomal stability were determined by using our previous published methods properties.[23]

Microsomal Stability. GIBIO pooled human liver microsomes (HLM) (Cat # HMMCPL), mouse liver microsomes (MLM) (Cat # BCMCPL), and rat liver microsomes (RLM) (Cat # RTMCPL) were purchased from Life Technologies. The incubations consisted of test compound (5 μM) or control compounds (verapamil and dextromethorphan), 0.5 mg/mL of microsomes, 3.3 mM $MgCl_2$, 1.3 mM β-NADPH, and 100 mM potassium phosphate buffer (pH 7.4). Samples are incubated at different time points up to 60 min. Reaction was terminated with ice-cold acetonitrile 0.3% formic acid. Samples were subsequently centrifuged at 4 ^{o}C for 15 min at 20,000×*g*. The supernatant was analyzed by LC–MS.

Pharmacokinetics (PK) and Tissue Distribution. [60, 61] All animal studies were done as per approved protocols by the Institutional Animal Care and Use Committee at the Biological Resource Centre (BRC) in Singapore. BALB/c mice or tumor bearing NCR nude mice were dosed iv, po, and ip with a variety of formulated solutions or suspensions of compound examples. Blood was collected after serial bleeding and centrifuged, and the plasma was frozen at −80°C. Tissues (e.g., livers, lungs, and kidney) were snap frozen on dry ice or in liquid nitrogen and kept at −80 °C until analysis. The plasma samples were added internal standard carbamazepine (CBZ) and processed as described previously.[61] Quantitative analysis was carried out on a Waters 2795 separations module equipped with a Waters 2996 Photodiode Array (PDA) detector and Micromass Quattro micro mass spectrometer. Sample was resolved on Phenomenex Luna C18(2), 2.0×50 mm column with a SecurityGuard Cartridge (C18 4×2.0 mm) at a flow of 0.5 mL/min with a 6-min gradient (x to 95% of B, solvent A, ultrapure water with 0.1% of formic acid (FA), solvent B, methanol with 0.1% of FA, x is selected from 5 to 50) and data

were acquired using multiple reaction monitoring and quantified by QuanLynx in MasLynx software (V 4.1, Waters Inc.).

In Vivo Pharmacodynamics (PD) and Efficacy Studies. All animal studies were done as per approved protocols by the Institutional Animal Care and Use Committee at the Biological Resource Centre (BRC) in Singapore. Female NCr nude mice (CrTac:NCr-*Foxn1*^{nu}), or BALB/c nude mice, or C.B-17 scid mice (C.B-Igh-1^{b}/IcrTac-Prkdc^{scid}), 4 to 6 weeks of age, purchased from InVivos Pte Ltd, Singapore, were inoculated in the right flank with about 5×10^6 of tumor cells which were suspended in serum-free DMEM or RPMI1640 growth medium and Matrigel (Cat. No: 354234, Corning Discovery Labware) (1:1) and injected in a total volume of 100 to 150 μL. Tumor were measured using a digital caliper and tumor volumes were estimated by using the formula: tumor volume = length × width^2 × 0.5. Tumor growth inhibition (TGI%) = [1 - (T_t - T_0)/(C_t - C_0)×100, C_0 and C_t are the mean tumor volumes for control group (vehicle) on day 0 and day t, respectively; T_0 and T_t are the mean tumor volumes for treatment group on day 0 and day t, respectively. All statistics conducted were done using GraphPad Prism (v4.00 or v7.00, GraphPad Software Inc.), two-tailed unpaired t-Test was used for comparing two groups, and one way ANOVA followed by Dunnett's Multiple Comparison Test was used for comparing three and more groups.

ASSOCIATED CONTENT

Supporting Information. The Supporting Information is available free of charge on the ACS Publications website at DOI: 10.1021/acs.jmedchem.xxxxx.

Source of reference compounds, supplementary Tables S1–S4, Figures S1–S2, synthesis of **20w**, anchorage-dependent clonogenic assay and soft agar colony formation assay, and molecular docking studies (PDF)

Molecular formula strings and some data (CSV)

AUTHOR INFORMATION

Corresponding Author

*Email: mcbwhs@gmail.com. Phone: +65-98265986. Fax: +65-62261209.

ORCID

Haishan Wang: 0000-0002-7959-7377

Wei Huang Goh: 0000-0001-9686-3713

Present Addresses

Author Contributions

Funding Sources

The project was supported by the Institute of Molecular and Cell Biology, Agency for Science, Technology and Research, Republic of Singapore.

Notes

HW, DC and CKS are inventors of patent applications associated with this publication. The authors declare no competing financial interest.

ACKNOWLEDGMENT

The authors thank the Institute of Molecular and Cell Biology for financial support, Xiaoli Xu (IMCB) for performing part of the animal work, Drs. Ken Chi Lik Lee and Li Yan Chan (Singapore Polytechnic) for providing NMR facility support, Dr. Manikanden Lakshmanan (IMCB) for ordering animals, Professor Wanjin Hong (IMCB) for valuable recommendations, the Experimental Therapeutics Centre (ETC) for supporting part of the outsourced enzymatic profiling work, interns from Singapore Polytechnic and Nanyang Polytechnic for chemical synthesis of the intermediates, and Zilong Wang for his help with the manuscript.

ABBREVIATIONS

AcH3, acetyl histone H3; Cl, clearance; HLM, human liver microsomes; MLM, mouse liver microsomes; RLM, rat liver microsomes; TGI, tumor growth inhibition; ZBG, zinc binding group.

REFERENCES

1. Development history and FDA approval process for Nexavar. https://www.drugs.com/history/nexavar.html (accessed Aug 15, 2017).

2. Lencioni, R.; Llovet, J. M. Modified RECIST (mRECIST) assessment for hepatocellular carcinoma. *Semin. Liver Dis.* **2010,** *30*, 052–060.

3. Development history and FDA approval process for stivarga. https://www.drugs.com/history/stivarga.html (accessed Aug 18, 2017).

4. Llovet, J. M. Regorafenib in second-line setting for hepatocellular carcinoma: balancing benefit with toxicity. http://www.ascopost.com/issues/february-25-2017/regorafenib-in-second-line-setting-for-hepatocellular-carcinoma-balancing-benefit-with-toxicity/ (accessed Aug 18, 2017).

5. Zhu, A. X.; Kudo, M.; Assenat, E.; Cattan, S.; Kang, Y.-K.; Lim, H. Y.; Poon, R. T. P.; Blanc, J.-F.; Vogel, A.; Chen, C.-L.; Dorval, E.; Peck-Radosavljevic, M.; Santoro, A.; Daniele, B.; Furuse, J.; Jappe, A.; Perraud, K.; Anak, O.; Sellami, D. B.; Chen, L.-T. Effect of everolimus on survival in advanced hepatocellular carcinoma after failure of sorafenib: the evolve-1 randomized clinical trial. *J. Am. Med. Assoc.* **2014,** *312*, 57–67.

6. Ler, S. Y.; Leung, C. H. W.; Khin, L. W.; Lu, G.-D.; Salto-Tellez, M.; Hartman, M.; Iau, P. T. C.; Yap, C. T.; Hooi, S. C. HDAC1 and HDAC2 independently predict mortality in hepatocellular carcinoma by a competing risk regression model in a southeast asian population. *Oncol. Rep.* **2015,** *34*, 2238–2250.

7. Wu, L.-M.; Yang, Z.; Zhou, L.; Zhang, F.; Xie, H.-Y.; Feng, X.-W.; Wu, J.; Zheng, S.-S. Identification of histone deacetylase 3 as a biomarker for tumor recurrence following liver transplantation in HBV-associated hepatocellular carcinoma. *PLoS One* **2011,** *5*, e14460.

8. Rikimaru, T.; Taketomi, A.; Yamashita, Y.; Shirabe, K.; Hamatsu, T.; Shimada, M.; Maehara, Y. Clinical significance of histone deacetylase 1 expression in patients with hepatocellular carcinoma. *Oncology* **2007,** *72*, 69–74.

9. Quint, K.; Agaimy, A.; Di Fazio, P.; Montalbano, R.; Steindorf, C.; Jung, R.; Hellerbrand, C.; Hartmann, A.; Sitter, H.; Neureiter, D.; Ocker, M. Clinical significance of histone deacetylases 1, 2, 3, and 7: HDAC2 is an independent predictor of survival in HCC. *Virchows Arch.* **2011,** *459*, 129–139.

10. Zhai, B.; Sun, X.-Y. Mechanisms of resistance to sorafenib and the corresponding strategies in hepatocellular carcinoma. *World J. Hepatol.* **2013,** *5*, 345–352.

11. Janku, F.; Kaseb, A. O.; Tsimberidou, A. M.; Wolff, R. A.; Kurzrock, R. Identification of novel therapeutic targets in the PI3K/AKT/mTOR pathway in hepatocellular carcinoma using targeted next generation sequencing. *Oncotarget* **2014,** *5*, 3012–3022.

12. Li, X.; Tao, J.; Cigliano, A.; Sini, M.; Calderaro, J.; Azoulay, D.; Wang, C.; Liu, Y.; Jiang, L.; Evert, K.; Demartis, M. I.; Ribback, S.; Utpatel, K.; Dombrowski, F.; Evert, M.; Calvisi, D. F.; Chen, X. Co-activation of PIK3CA and Yap promotes development of hepatocellular and cholangiocellular tumors in mouse and human liver. *Oncotarget* **2015,** *6*, 10102–10115.

13. Chen, K.-F.; Chen, H.-L.; Tai, W.-T.; Feng, W.-C.; Hsu, C.-H.; Chen, P.-J.; Cheng, A.-L. Activation of phosphatidylinositol 3-kinase/Akt signaling pathway mediates acquired resistance to sorafenib in hepatocellular carcinoma cells. *J. Pharmacol. Exp. Ther.* **2011,** *337*, 155–161.

14. Bitzer, M.; Horger, M.; Giannini, E. G.; Ganten, T. M.; Wörns, M. A.; Siveke, J. T.; Dollinger, M. M.; Gerken, G.; Scheulen, M. E.; Wege, H.; Zagonel, V.; Cillo, U.; Trevisani, F.; Santoro, A.; Montesarchio, V.; Malek, N. P.; Holzapfel, J.; Herz, T.; Ammendola, A. S.;

Pegoraro, S.; Hauns, B.; Mais, A.; Lauer, U. M.; Henning, S. W.; Hentsch, B. Resminostat plus sorafenib as second-line therapy of advanced hepatocellular carcinoma – The SHELTER study. *J. Hepatol.* **2016,** *65*, 280–288.

15. Lu, Y.-S.; Kashida, Y.; Kulp, S. K.; Wang, Y.-C.; Wang, D.; Hung, J.-H.; Tang, M.; Lin, Z.-Z.; Chen, T.-J.; Cheng, A.-L.; Chen, C.-S. Efficacy of a novel histone deacetylase inhibitor in murine models of hepatocellular carcinoma. *Hepatology* **2007,** *46*, 1119–1130.

16. Lachenmayer, A.; Toffanin, S.; Alsinet, L. C. C.; Hoshida, Y.; Minguez, A. V. B.; Tsai, H.-W.; Ward, S. C.; Thung, S.; Friedman, S. L.; Llovet, J. M. Combination therapy for hepatocellular carcinoma: additive preclinical efficacy of the HDAC inhibitor panobinostat with sorafenib. *J. Hepatol.* **2012,** *56*, 1343–1350.

17. Yeo, W.; Chung, H. C.; Chan, S. L.; Wang, L. Z.; Lim, R.; Picus, J.; Boyer, M.; Mo, F. K. F.; Koh, J.; Rha, S. Y.; Hui, E. P.; Jeung, H. C.; Roh, J. K.; Yu, S. C. H.; To, K. F.; Tao, Q.; Ma, B. B.; Chan, A. W. H.; Tong, J. H. M.; Erlichman, C.; Chan, A. T. C.; Goh, B. C. Epigenetic therapy using belinostat for patients with unresectable hepatocellular carcinoma: a multicenter phase I/II study with biomarker and pharmacokinetic analysis of tumors from patients in the Mayo phase II consortium and the cancer therapeutics research group. *J. Clin. Oncol.* **2012,** *30*, 3361–3367.

18. Somoza, J. R.; Koditek, D.; Villaseñor, A. G.; Novikov, N.; Wong, M. H.; Liclican, A.; Xing, W.; Lagpacan, L.; Wang, R.; Schultz, B. E.; Papalia, G. A.; Samuel, D.; Lad, L.; McGrath, M. E. Structural, biochemical, and biophysical characterization of idelalisib binding to phosphoinositide 3-kinase δ. *J. Biol. Chem.* **2015,** *290*, 8439–8446.

19. Scott, W. J.; Hentemann, M. F.; Rowley, R. B.; Bull, C. O.; Jenkins, S.; Bullion, A. M.; Johnson, J.; Redman, A.; Robbins, A. H.; Esler, W.; Fracasso, R. P.; Garrison, T.; Hamilton, M.;

Michels, M.; Wood, J. E.; Wilkie, D. P.; Xiao, H.; Levy, J.; Stasik, E.; Liu, N.; Schaefer, M.; Brands, M.; Lefranc, J. Discovery and SAR of novel 2,3-dihydroimidazo[1,2-c]quinazoline PI3K Inhibitors: identification of copanlisib (BAY 80-6946). *ChemMedChem* **2016,** *11*, 1517–1530.

20. Shao, H.; Gao, C.; Tang, H.; Zhang, H.; Roberts, L. R.; Hylander, B. L.; Repasky, E. A.; Ma, W. W.; Qiu, J.; Adjei, A. A.; Dy, G. K.; Yu, C. Dual targeting of mTORC1/C2 complexes enhances histone deacetylase inhibitor-mediated anti-tumor efficacy in primary HCC cancer in vitro and in vivo. *J. Hepatol.* **2012,** *56*, 176–183.

21. Gedaly, R.; Angulo, P.; Hundley, J.; Daily, M. F.; Chen, C.; Evers, B. M. PKI-587 and sorafenib targeting PI3K/AKT/mTOR and Ras/Raf/MAPK pathways synergistically inhibit HCC cell proliferation. *J. Surg. Res.* **2012,** *176*, 542–548.

22. Wang, H.; Yu, N.; Song, H.; Chen, D.; Zou, Y.; Deng, W.; Lye, P. L.; Chang, J.; Ng, M.; Blanchard, S.; Sun, E. T.; Sangthongpitag, K.; Wang, X.; Goh, K. C.; Wu, X.; Khng, H. H.; Fang, L.; Goh, S. K.; Ong, W. C.; Bonday, Z.; Stünkel, W.; Poulsen, A.; Entzeroth, M. N-Hydroxy-1,2-disubstituted-1H-benzimidazol-5-yl acrylamides as novel histone deacetylase inhibitors: design, synthesis, SAR studies, and in vivo antitumor activity. *Bioorg. Med. Chem. Lett.* **2009,** *19*, 1403–1408.

23. Wang, H.; Lim, Z.-Y.; Zhou, Y.; Ng, M.; Lu, T.; Lee, K.; Sangthongpitag, K.; Goh, K. C.; Wang, X.; Wu, X.; Khng, H. H.; Goh, S. K.; Ong, W. C.; Bonday, Z.; Sun, E. T. Acylurea connected straight chain hydroxamates as novel histone deacetylase inhibitors: synthesis, SAR, and in vivo antitumor activity. *Bioorg. Med. Chem. Lett.* **2010,** *20*, 3314–3321.

24. Wang, H.; Yu, N.; Chen, D.; Lee, K. C. L.; Lye, P. L.; Chang, J. W. W.; Deng, W.; Ng, M. C. Y.; Lu, T.; Khoo, M. L.; Poulsen, A.; Sangthongpitag, K.; Wu, X.; Hu, C.; Goh, K. C.; Wang, X.; Fang, L.; Goh, K. L.; Khng, H. H.; Goh, S. K.; Yeo, P.; Liu, X.; Bonday, Z.; Wood, J.

M.; Dymock, B. W.; Kantharaj, E.; Sun, E. T. Discovery of (2E)-3-{2-butyl-1-[2-(diethylamino)ethyl]-1H-benzimidazol-5-yl}-N-hydroxyacrylamide (SB939), an orally active histone deacetylase inhibitor with a superior preclinical profile. *J. Med. Chem.* **2011,** *54*, 4694–4720.

25. Hart, S.; Novotny-Diermayr, V.; Goh, K. C.; Williams, M.; Tan, Y. C.; Ong, L. C.; Cheong, A.; Ng, B. K.; Amalini, C.; Madan, B.; Nagaraj, H.; Jayaraman, R.; Pasha, K. M.; Ethirajulu, K.; Chng, W. J.; Mustafa, N.; Goh, B. C.; Benes, C.; McDermott, U.; Garnett, M.; Dymock, B.; Wood, J. M. VS-5584, a novel and highly selective PI3K/mTOR kinase inhibitor for the treatment of cancer. *Mol. Cancer Ther.* **2013,** *12*, 151–161.

26. Poulsen, A.; Nagaraj, H.; Lee, A.; Blanchard, S.; Soh, C. K.; Chen, D.; Wang, H.; Hart, S.; Goh, K. C.; Dymock, B.; Williams, M. Structure and ligand-based design of mTOR and PI3-kinase inhibitors leading to the clinical candidates VS-5584 (SB2343) and SB2602. *J. Chem. Inf. Model.* **2014,** *54*, 3238–3250.

27. Wang, H.; Chen, D.; Soh, C. K. Fused Pyrimidine-based Hydroxamate Derivatives. PCT Int. Appl. WO2015137887A1, September 17, 2015.

28. Finnin, M.; Donigian, J.; Cohen, A.; Richon, V.; Rifkind, R.; Marks, P.; Breslow, R.; Pavletich, N. Structures of a histone deacetylase homologue bound to the TSA and SAHA inhibitors. *Nature* **1999,** *401*, 188–193.

29. Wang, H.; Dymock, B. W. New patented histone deacetylase inhibitors. *Expert Opin.Ther. Pat.* **2009,** *19*, 1727–1757.

30. Raynaud, F. I.; Eccles, S. A.; Patel, S.; Alix, S.; Box, G.; Chuckowree, I.; Folkes, A.; Gowan, S.; De Haven Brandon, A.; Di Stefano, F.; Hayes, A.; Henley, A. T.; Lensun, L.; Pergl-Wilson, G.; Robson, A.; Saghir, N.; Zhyvoloup, A.; McDonald, E.; Sheldrake, P.; Shuttleworth,

S.; Valenti, M.; Wan, N. C.; Clarke, P. A.; Workman, P. Biological properties of potent inhibitors of class I phosphatidylinositide 3-kinases: from PI-103 through PI-540, PI-620 to the oral agent GDC-0941. *Mol. Cancer Ther.* **2009,** *8*, 1725–1738.

31. Folkes, A. J.; Ahmadi, K.; Alderton, W. K.; Alix, S.; Baker, S. J.; Box, G.; Chuckowree, I. S.; Clarke, P. A.; Depledge, P.; Eccles, S. A.; Friedman, L. S.; Hayes, A.; Hancox, T. C.; Kugendradas, A.; Lensun, L.; Moore, P.; Olivero, A. G.; Pang, J.; Patel, S.; Pergl-Wilson, G. H.; Raynaud, F. I.; Robson, A.; Saghir, N.; Salphati, L.; Sohal, S.; Ultsch, M. H.; Valenti, M.; Wallweber, H. J.; Wan, N. C.; Wiesmann, C.; Workman, P.; Zhyvoloup, A.; Zvelebil, M. J.; Shuttleworth, S. J. The identification of 2-(1H-indazol-4-yl)-6-(4-methanesulfonyl-piperazin-1-ylmethyl)-4-morpholin-4-yl-thieno[3,2-d]pyrimidine (GDC-0941) as a potent, selective, orally bioavailable inhibitor of class I PI3 kinase for the treatment of cancer. *J. Med. Chem.* **2008,** *51*, 5522–5532.

32. Sarker, D.; Ang, J. E.; Baird, R.; Kristeleit, R.; Shah, K.; Moreno, V.; Clarke, P. A.; Raynaud, F. I.; Levy, G.; Ware, J. A.; Mazina, K.; Lin, R.; Wu, J.; Fredrickson, J.; Spoerke, J. M.; Lackner, M. R.; Yan, Y.; Friedman, L. S.; Kaye, S. B.; Derynck, M. K.; Workman, P.; de Bono, J. S. First-in-human phase I study of pictilisib (GDC-0941), a potent pan-class I phosphatidylinositol-3-kinase (PI3K) inhibitor, in patients with advanced solid tumors. *Clin. Cancer Res.* **2015,** *21*, 77–86.

33. Richardson, P. G. Dual inhibition of oncogenic targets for B-cell malignancies. *Lancet Oncol.* **2016,** *17*, 547–549.

34. Younes, A.; Berdeja, J. G.; Patel, M. R.; Flinn, I.; Gerecitano, J. F.; Neelapu, S. S.; Kelly, K. R.; Copeland, A. R.; Akins, A.; Clancy, M. S.; Gong, L.; Wang, J.; Ma, A.; Viner, J. L.; Oki, Y. Safety, tolerability, and preliminary activity of CUDC-907, a first-in-class, oral, dual inhibitor

of HDAC and PI3K, in patients with relapsed or refractory lymphoma or multiple myeloma: an open-label, dose-escalation, phase 1 trial. *Lancet Oncol.* **2016,** *17*, 622–631.

35. Cai, X.; Zhai, H.; Lai, C.; Qian, C.; Bao, R. Phosphoinositide 3-Kinase Inhibitor with a Zinc Binding Moiety. U.S. Patent 8,710,219 B2, April 29, 2014.

36. Qian, C.; Lai, C.-J.; Bao, R.; Wang, D.-G.; Wang, J.; Xu, G.-X.; Atoyan, R.; Qu, H.; Yin, L.; Samson, M.; Zifcak, B.; Ma, A. W. S.; DellaRocca, S.; Borek, M.; Zhai, H.-X.; Cai, X.; Voi, M. Cancer network disruption by a single molecule inhibitor targeting both histone deacetylase activity and phosphatidylinositol 3-kinase signaling. *Clin. Cancer Res.* **2012,** *18*, 4104–4113.

37. Flinn, I. W.; Oki, Y.; Copland, A.; Fattaey, A.; Lai, C.-J.; Laliberte, R.; Voi, M.; Berdeja, J. G. A first-in-man phase 1 study of CUDC-907, a first-in-class chemically-designed dual inhibitor of PI3K and HDAC in patients with refractory or relapsed lymphoma and multiple myeloma. *Blood* **2013,** *122*, 4363–4363.

38. Venugopal, B.; Baird, R.; Kristeleit, R. S.; Plummer, R.; Cowan, R.; Stewart, A.; Fourneau, N.; Hellemans, P.; Elsayed, Y.; Mcclue, S.; Smit, J. W.; Forslund, A.; Phelps, C.; Camm, J.; Evans, T. R. J.; de Bono, J. S.; Banerji, U. A phase I study of quisinostat (JNJ-26481585), an oral hydroxamate histone deacetylase inhibitor with evidence of target modulation and antitumor activity, in patients with advanced solid tumors. *Clin. Cancer Res.* **2013,** *19*, 4262–4272.

39. Child, F.; Ortiz-Romero, P. L.; Alvarez, R.; Bagot, M.; Stadler, R.; Weichenthal, M.; Alves, R.; Quaglino, P.; Beylot-Barry, M.; Cowan, R.; Geskin, L. J.; Pérez-Ferriols, A.; Hellemans, P.; Elsayed, Y.; Phelps, C.; Forslund, A.; Kamida, M.; Zinzani, P. L. Phase II multicentre trial of oral quisinostat, a histone deacetylase inhibitor, in patients with previously treated stage IB–IVA mycosis fungoides/Sézary syndrome. *Br. J. Dermatol.* **2016**, *175*, 80–88.

40. Andrs, M.; Korabecny, J.; Jun, D.; Hodny, Z.; Bartek, J.; Kuca, K. Phosphatidylinositol 3-kinase (PI3K) and phosphatidylinositol 3-kinase-related kinase (PIKK) Inhibitors: importance of the morpholine ring. *J. Med. Chem.* **2015,** *58*, 41–71.

41. Trott, O.; Olson, A. J. AutoDock Vina: Improving the speed and accuracy of docking with a new scoring function, efficient optimization, and multithreading. *J. Comput. Chem.* **2010,** *31*, 455–461.

42. Zhao, Y.; Zhang, X.; Chen, Y.; Lu, S.; Peng, Y.; Wang, X.; Guo, C.; Zhou, A.; Zhang, J.; Luo, Y.; Shen, Q.; Ding, J.; Meng, L.; Zhang, J. Crystal structures of PI3Kα complexed with PI103 and Its derivatives: new directions for inhibitors design. *ACS Med. Chem. Lett.* **2014,** *5*, 138–142.

43. Frew, A. J.; Johnstone, R. W.; Bolden, J. E. Enhancing the apoptotic and therapeutic effects of HDAC inhibitors. *Cancer Lett.* **2009,** *280*, 125–133.

44. van Malenstein, H.; Dekervel, J.; Verslype, C.; Van Cutsem, E.; Windmolders, P.; Nevens, F.; van Pelt, J. Long-term exposure to sorafenib of liver cancer cells induces resistance with epithelial-to-mesenchymal transition, increased invasion and risk of rebound growth. *Cancer Lett.* **2013,** *329*, 74–83.

45. Gedaly, R.; Angulo, P.; Chen, C. C., K T; Spear, B. T.; Hundley, J.; Daily, M. F.; Shah, M.; Evers, B. M. The role of PI3K/mTOR inhibition in combination with sorafenib in hepatocellular carcinoma treatment. *Anticancer Res.* **2012,** *32*, 2531–2536.

46. Yeo, P.; Xin, L.; Goh, E.; New, L. S.; Zeng, P.; Wu, X.; Venkatesh, P.; Kantharaj, E. Development and validation of high-performance liquid chromatography–tandem mass spectrometry assay for 6-(3-benzoyl-ureido)-hexanoic acid hydroxyamide, a novel HDAC

inhibitor, in mouse plasma for pharmacokinetic studies. *Biomed. Chromatogr.* **2007,** *21*, 184–189.

47. National Cancer Centre Singapore (NCCS). Signature programme : liver cancer. https://www.nccs.com.sg/Research/programmes/Signature/Pages/LiverCancer.aspx (accessed Nov 18, 2017).

48. Ikeda, M.; Mitsunaga, S.; Ohno, I.; Hashimoto, Y.; Takahashi, H.; Watanabe, K.; Umemoto, K.; Okusaka, T. Systemic chemotherapy for advanced hepatocellular carcinoma: past, present, and future. *Diseases* **2015,** *3*, 360–381.

49. Chen, Y.; Wang, X.; Xiang, W.; He, L.; Tang, M.; Wang, F.; Wang, T.; Yang, Z.; Yi, Y.; Wang, H.; Niu, T.; Zheng, L.; Lei, L.; Li, X.; Song, H.; Chen, L. Development of purine-based hydroxamic acid derivatives: potent histone deacetylase inhibitors with marked in vitro and in vivo antitumor activities. *J. Med. Chem.* **2016,** *59*, 5488–5504.

50. Bristol-Myers Squibb's opdivo (nivolumab) receives FDA approval for the treatment of hepatocellular carcinoma patients previously treated with sorafenib. https://www.drugs.com/newdrugs/bristol-myers-squibb-s-opdivo-nivolumab-receives-fda-approval-hepatocellular-carcinoma-patients-4607.html (accessed Sep 22, 2017).

51. Shen, L.; Ciesielski, M.; Ramakrishnan, S.; Miles, K. M.; Ellis, L.; Sotomayor, P.; Shrikant, P.; Fenstermaker, R.; Pili, R. Class I histone deacetylase inhibitor entinostat suppresses regulatory T cells and enhances immunotherapies in renal and prostate cancer models. *PLoS One* **2012,** *7*, e30815.

52. Yardley, D. A.; Ismail-Khan, R. R.; Melichar, B.; Lichinitser, M.; Munster, P. N.; Klein, P. M.; Cruickshank, S.; Miller, K. D.; Lee, M. J.; Trepel, J. B. Randomized phase II, double-blind, placebo-controlled study of exemestane with or without entinostat in postmenopausal

women with locally recurrent or metastatic estrogen receptor-positive breast cancer progressing on Treatment With a Nonsteroidal Aromatase Inhibitor. *J. Clin. Oncol.* **2013,** *31*, 2128–2135

53. Wardley, A. M. Phase II data for entinostat, a class 1 selective histone deacetylase inhibitor, in patients whose breast cancer is progressing on aromatase inhibitor therapy [abstract]. *J. Clin. Oncol.* **2010,** *28*, a1052.

54. Hooker, J. M.; Kim, S. W.; Alexoff, D.; Xu, Y.; Shea, C.; Reid, A.; Volkow, N.; Fowler, J. S. Histone deacetylase inhibitor MS-275 exhibits poor brain penetration: pharmacokinetic studies of [(11)C]MS-275 using positron emission tomography. *ACS Chem. Neurosci.* **2010,** *1*, 65–73.

55. Kim, H. M.; Han, S. B.; Kim, M. S.; Kang, J. S.; Oh, G. T.; Hong, D. H. Efficient fixation procedure of human leukemia cells in sulforhodamine B cytotoxicity assay. *J. Pharmacol. Toxicol. Methods* **1996,** *36*, 163–169.

56. Vichai, V.; Kirtikara, K. Sulforhodamine B colorimetric assay for cytotoxicity screening. *Nat. Protoc.* **2006,** *1*, 1112–1116.

57. Promega Corporation. CellTiter-Glo® luminescent cell viability assay. https://www.promega.sg/~/media/Files/Resources/Protocols/Technical%20Bulletins/0/CellTiter%20Glo%20Luminescent%20Cell%20Viability%20Assay%20Protocol.pdf (accessed Dec 9, 2015).

58. Lorenzi, P. L.; Reinhold, W. C.; Varma, S.; Hutchinson, A. A.; Pommier, Y.; Chanock, S. J.; Weinstein, J. N. DNA fingerprinting of the NCI-60 cell line panel. *Mol. Cancer Ther.* **2009,** *8*, 713–724.

59. Huang, Y.; Liu, Y.; Zheng, C.; Shen, C. Investigation of cross-contamination and misidentification of 278 widely used tumor cell lines. *PLoS ONE* **2017,** *12*, e0170384.

60. Venkatesh, P. R.; Goh, E.; Zeng, P. Z.; New, L. S.; Xin, L.; Pasha, M. K.; Sangthongpitag, K.; Yeo, P.; Kantharaj, E. In vitro phase I cytochrome P450 metabolism, permeability and pharmacokinetics of SB639, a novel histone deacetylase inhibitor in preelinical species. *Biol. Pharm. Bull.* **2007,** *30*, 1021–1024.

61. Jayaraman, R.; Reddy, V. P.; Pasha, M. K.; Wang, H.; Sangthongpitag, K.; Yeo, P.; Hu, C. Y.; Wu, X.; Xin, L.; Goh, E.; New, L. S.; Ethirajulu, K. Preclinical metabolism and disposition of SB939 (Pracinostat), an orally active histone deacetylase (HDAC) inhibitor, and prediction of human pharmacokinetics. *Drug Metab. Dispos.* **2011,** *39*, 2219–2232.

Table of Contents Graphic